

ACTIVE VIBRATION CONTROL OF A SMART SANDWICH PLATE VIA
PIEZOELECTRIC SENSORS AND ACTUATORS

A THESIS SUBMITTED TO
THE GRADUATE SCHOOL OF NATURAL AND APPLIED SCIENCES
OF
MIDDLE EAST TECHNICAL UNIVERSITY

BY

YUNUS TANSU AKSOY

IN PARTIAL FULFILLMENT OF THE REQUIREMENTS
FOR
THE DEGREE OF MASTER OF SCIENCE
IN
AEROSPACE ENGINEERING

SEPTEMBER 2015

Approval of the thesis:

**ACTIVE VIBRATION CONTROL OF SANDWICH PLATES VIA
PIEZOELECTRIC SENSORS AND ACTUATORS**

submitted by **YUNUS TANSU AKSOY** in partial fulfilment of the requirements for
the degree of **Master of Science in Aerospace Engineering Department, Middle
East Technical University** by,

Prof. Dr. Gülbin Dural Ünver _____
Director, Graduate School of **Natural and Applied Sciences**

Prof. Dr. Ozan Tekinalp _____
Head of Department, **Aerospace Engineering**

Assoc. Prof. Dr. Melin Şahin _____
Supervisor, **Aerospace Engineering Dept., METU**

Examining Committee Members:

Prof. Dr. Yavuz Yaman _____
Aerospace Engineering Dept., METU

Assoc. Prof. Dr. Melin Şahin _____
Aerospace Engineering Dept., METU

Assist. Prof. Dr. Ercan Gürses _____
Aerospace Engineering Dept., METU

Assist. Prof. Dr. A. Türker Kutay _____
Aerospace Engineering Dept., METU

Prof. Dr. Metin U. Salamcı _____
Mechanical Engineering Dept., Gazi University

Date: 02.09.2015

I hereby declare that all the information in this document has been obtained and presented in accordance with academic rules and ethical conduct. I also declare that, as required by these rules and conduct, I have fully cited and referenced all material and results that are not original to this work.

Name, Last Name:

Signature:

ABSTRACT

ACTIVE VIBRATION CONTROL OF A SMART SANDWICH PLATE VIA PIEZOELECTRIC SENSORS AND ACTUATORS

Aksoy, Yunus Tansu

M.S., Department of Aerospace Engineering

Supervisor : Assoc. Prof. Dr. Melin Şahin

September 2015, 85 pages

In this study, the first three vibration modes of a smart sandwich plate, which are 1st out-of-plane bending, 1st torsion and 2nd out-of-plane bending modes, are aimed to be suppressed by using active vibration control techniques comprising a pole placement controller. Smart sandwich plate is composed of a passive sandwich composite plate and piezoelectric patches (PZT Lead-Zirconate-Titanate) attached with epoxy adhesive at specific locations determined by using finite element modelling and analysis. Those PZT patches on the smart sandwich plate are then used both as actuators and sensors.

Before manufacturing the smart sandwich plate, the locations of PZT patches are determined by considering the vibrational characteristics of the sandwich plate. Following this, an experimental modal analysis is performed to verify the finite element analysis results. Additionally, the model is updated according to the experimental results. Then, an algorithm is adapted in order to determine the spatial locations of the PZT patches and parallel to the obtained results they are attached to the passive sandwich plate. After the manufacturing process of the smart sandwich plate, a system identification is performed experimentally by sending an input signal covering the frequencies of interest and recording the response through a designated

sensor. Having obtained the frequency response function of the smart sandwich plate experimentally, a transfer function is fitted in the frequency domain.

Finally, various active vibration controllers are designed. Those controllers are then validated through simulations and applied in an experimental environment via pole placement method combined with various observers and filters to suppress the free and forced vibrations of the smart sandwich plate at the aforementioned resonance frequencies. The three different designed controllers are observed to suppress the vibrations in each of the aimed mode successfully by working individually and also operating together without compromising the individual performance of the controllers in the vibration suppression of the smart sandwich plate.

Keywords: Active Vibration Control, Frequency Response Functions, Finite Element Method, Piezoelectric Materials, Smart Sandwich Plate

ÖZ

AKILLI BİR SANDVIÇ PLAKANIN PİEZOELEKTRİK UYARICILAR VE ALGILAYICILAR YARDIMIYLA AKTİF TİTREŞİM KONTROLÜ

Aksoy, Yunus Tansu

Yüksek Lisans, Havacılık ve Uzay Mühendisliği Bölümü

Tez Yöneticisi : Doç. Dr. Melin Şahin

Eylül 2015, 85 sayfa

Bu çalışmada, akıllı sandviç plakanın düzleme dik ilk eğilme, ilk burulma ve düzleme dik ikinci eğilme olan ilk üç titreşim modunun kutup yerleşim metodu kullanılarak aktif titreşim kontrolü teknikleriyle bastırılması amaçlanmıştır. Akıllı sandviç plaka, sonlu elemanlar yöntemiyle yerleri belirlenmiş, epoksi yapıştırıcı ile bağlanmış piezoelektrik yamalardan ve pasif bir kompozit plakadan oluşmaktadır. Akıllı sandviç plaka üzerindeki piezoelektrik yamalar hem uyarıcı hem de algılayıcı olarak kullanılmışlardır.

Akıllı sandviç plakanın üretiminden önce, sandviç plakanın titreşim özellikleri değerlendirilerek piezoelektrik yamaların yerleri belirlenmiştir. Ardından, deneysel modal analizler yapılarak sonlu elemanlar analiz sonuçları da doğrulanmıştır. Buna ilave olarak deney sonuçlarına göre model güncellemeleri tamamlanmış ve piezoelektrik yamaların yerlerini belirlemek için bir algoritma uygulanmak suretiyle elde edilen sonuçlara paralel olarak bu yamalar pasif sandviç plakaya yapıştırılmıştır. Akıllı sandviç plakanın üretim işleminin ardından, ilgili olan frekansları içeren bir girdi sinyaliyle ve belirlenen algılayıcının yanıtıyla deneysel sistem tanılaması tamamlanmıştır. Akıllı sandviç plakanın frekans cevap fonksiyonunun deneysel yöntemle elde edilmesiyle, frekans kümesinde bir transfer fonksiyonu uyarlanmıştır.

Son olarak, akıllı sandviç plakanın yukarıda bahsedilen rezonans frekanslarında, serbest ve zorlanmış titreşimleri bastırmak için çeşitli gözlemci ve filtrelerle kombine edilmiş kutup yerleşim metotlu aktif titreşim kontrolcöleri tasarlanmış, benzetimlerle doğrulanmış ve deneysel ortamda uygulanmıştır. Üç farklı kontrolcünün, akıllı sandviç plakanın amaçlanan her modundaki titreşimleri tek tek bastırmakta başarı göstermiş olduğu ve bu tekil performanslarından çok da ödün vermeden bir arada da çalıştıkları gözlenmiştir.

Anahtar Kelimeler: Aktif Titreşim Kontrolü, Frekans Cevap Fonksiyonları, Sonlu Eleman Modelleri, Piezoelektrik Malzemeler, Akıllı Sandviç Plaka

To
My fiancée
And
My family

ACKNOWLEDGMENTS

I would like to express my greatest gratitude to my supervisor Assoc. Prof. Dr. Melin ŞAHİN, for giving me an opportunity to work with him, allowing me to benefit from his invaluable comments and experiences and his endless patience throughout my study.

I would like to thank to Senior Engineers at ROKETSAN, Emre AÇMAZ and Barış AKGÜN and the General Manager of ODAK Kompozit Halil ŞENDİL for supplying the composite sandwich plate used in the thesis. I would also like to give my special thanks to Dr. Tayfun ÇİMEN and Arda AKSU for giving me supports about my thesis while I was working at ROKETSAN. I also want to give special thanks to Onur AKIN and Nima PEDRAMASL for helping me about the control and vibration theories and software and hardware used in the thesis. Thanks to Metehan YAYLA for helping about control theories. Additional thanks to my fiancée Pınar ENEREN for helping me about any topic throughout my thesis.

I also want to thank to all of my colleagues at ROKETSAN and METU for their friendship.

I want to give my thanks to my family and fiancée for their moral and material support.

I gratefully acknowledge the scientific research project BAP-03-13-2014-001 for the hardware and METUWIND for the software support and the SENSOR technology Ltd. for providing PZT patches, ODAK Kompozit Teknolojileri A.Ş for manufacturing the Sandwich Composite Plate and Edirne Karaçalı Torna for the boundary condition.

TABLE OF CONTENTS

ABSTRACT.....	v
ÖZ	vii
ACKNOWLEDGMENTS	x
TABLE OF CONTENTS	xi
LIST OF TABLES	xiii
LIST OF FIGURES	xiv
CHAPTERS	
1. INTRODUCTION	1
1.1 Background of the Study.....	2
1.1.1 Sandwich Structures	3
1.1.2 Piezoelectric Materials.....	4
1.1.3 Active Vibration Control	5
1.2 Motivation of the Thesis	6
1.3 Outline of the Thesis	6
2. MODAL ANALYSIS OF THE SANDWICH PLATE	9
2.1 Introduction	9
2.2 Finite Element Modelling and Analysis of the Sandwich Plate.....	9
2.3 Experimental Modal Analysis (EMA) of the Sandwich Plate	12
2.4 FEM Updating based on EMA Results.....	18
2.5 Conclusion.....	21
3. DETERMINATION OF THE ACTUATOR AND SENSOR LOCATIONS FOR THE SANDWICH PLATE.....	23
3.1 Introduction	23
3.2 Determination of the Location of the Piezoelectric Sensors	25
3.3 Determination of the Locations of the Piezoelectric Actuators	30
3.4 Conclusion.....	34

4. SYSTEM IDENTIFICATION OF THE SMART SANDWICH PLATE	35
4.1 Introduction	35
4.2 Experimental Setup	35
4.3 Mathematical Modelling of the Experimental System.....	37
4.3.1 Transfer Function between the 1 st Piezoelectric Actuator Patch Group and the Sensor	40
4.3.2 Transfer Function between the 2 nd Piezoelectric Actuator Patch Group and the Sensor	43
4.3.3 Transfer Function between the 3 rd Piezoelectric Actuator Patch Group and the Sensor	45
4.4 Conclusion.....	47
5. ACTIVE VIBRATION CONTROL OF THE SMART SANDWICH PLATE	49
5.1 Introduction	49
5.2 Design of the Active Vibration Controller	49
5.3 Simulations for Active Vibration Control	55
5.3.1 System Modelling of the Plant.....	55
5.3.2 Simulation Results of Active Vibration Control of the Smart Sandwich Plate.....	58
5.4 Case Study 1: Active Vibration Control of the Plate due to an Initial Condition: Free Vibration Suppression	64
5.5 Case Study 2: Active Vibration Control of the Plate due to an External Force: Force Vibration Suppression.....	65
5.5.1 Sinusoidal Signals at Resonant Frequencies.....	65
5.5.2 Sinusoidal Chirp Signal	72
5.6 Conclusion.....	75
6. CONCLUSIONS	77
6.1 General Conclusions.....	77
6.2 Recommendation for Future Work.....	78
REFERENCES.....	81

LIST OF TABLES

TABLES

Table 1.1 Honeycomb Sandwich Panel Structural Efficiency [22]	3
Table 2.1 Material Properties of SGL GE8903-280-37e Prepreg E-Glass	10
Table 2.2 Material Properties of Rohacell 31 IG-F Foam	10
Table 2.3 Natural and Resonance Frequencies of the Sandwich Plate	16
Table 2.4 MAC Matrix between FEA and EMA before Model Updating	19
Table 2.5 Updated Material Properties of SGL GE8903-280-37e Prepreg E-Glass..	19
Table 2.6 Natural Frequencies found by EMA and FEA before and after the Updating	20
Table 2.7 MAC Matrix between FEA and EMA after Model Updating	20
Table 4.1 Comparison of the Amplitude of the Resonant Peaks due to Excitation of Each Piezoelectric Actuator Group.....	48
Table 4.2 Comparison of the Resonance Frequencies before and after PZT Attachment	48
Table 5.1 Damping Ratio Multipliers for each of the Controller Group	52
Table 5.2 Gain Matrices of the Controllers and the Observers.....	53
Table 5.3 Simulated Attenuation Levels of Each Mode	63
Table 5.4 Free Vibration Suppression Durations	65
Table 5.5 Comparison of Attenuation Levels	75

LIST OF FIGURES

FIGURES

Figure 1.1 Generator and Motor Actions of a Piezoelectric Element: (a) disk after polarization, (b) disk compressed: generated voltage has some polarity as poling voltage, (c) disk stretched: generated voltage has polarity opposite that of poling voltage, (d) applied voltage has same polarity as poling voltage: disk lengthens, (e) applied voltage has polarity opposite that of poling [24]	4
Figure 2.1 Mesh Converge Plots (a) 1 st Natural Frequency, (b) 2 nd Natural Frequency, (c) 3 rd Natural Frequency	11
Figure 2.2 Natural Frequencies and the Corresponding Mode Shapes of the Sandwich Plate by FEA: (a) First Out-of-Plane Bending Mode [13.54 Hz], (b) First Torsional Mode [31.22 Hz], (c) Second Out-of-Plane Bending Mode [81.90 Hz]	12
Figure 2.3 Modal Analysis Test Equipment [47]: (a) B&K 6-Channel PULSE Data Acquisition System, (b) B&K 8206 Impact Hammer, (c) B&K 4517-002 Single Axis Accelerometer [46]	13
Figure 2.4 Modal Analysis Test Setup (Oblique View).....	14
Figure 2.5 Test Points on the Specimen	15
Figure 2.6 Stability Diagram of Point FRF	16
Figure 2.7 Resonance Frequencies and the corresponding Mode Shapes of the Sandwich Plate by EMA: (a) First out-of-Plane Bending Mode [11.53 Hz], (b) First Torsional Mode [33.94 Hz], (c) Second out-of-Plane Bending Mode [71.11 Hz].....	17
Figure 3.1 Sandwich Plate: (a) 1 st Mode Shape, (b) Curvature in x direction, (c) Curvature in y direction	26
Figure 3.2 Sandwich Plate: (a) 2 nd Mode Shape, (b) Curvature in x direction, (c) Curvature in y direction	27

Figure 3.3 Sandwich Plate: (a) 3 rd Mode Shape, (b) Curvature in x direction, (c) Curvature in y direction	28
Figure 3.4 Piezoelectric Patch (SensorTech - BM500 PZT Patch).....	29
Figure 3.5 Location of the Piezoelectric Patch as a Sensor	29
Figure 3.6 Flowchart of the Placement Algorithm	31
Figure 3.7 Locations of the Piezoelectric Patches for Disturbance and Sensor.....	32
Figure 3.8 Locations of the Piezoelectric Actuators	32
Figure 3.9 Locations of all Piezoelectric Patches	33
Figure 3.10 Smart Sandwich Plate	33
Figure 4.1 Smart Sandwich Plate	36
Figure 4.2 Experimental Setup Configuration	37
Figure 4.3 First 50 Seconds Time History of Input Signal	37
Figure 4.4 Response of the sensor to the 1 st Piezoelectric Actuator Patch Group in Time Domain	41
Figure 4.5 Frequency Response Function between the 1 st Piezoelectric Actuator Patch Group and the Sensor	41
Figure 4.6 FRF for the 1 st Piezoelectric Patch Group obtained by Mathematical Model and Experimental Data	42
Figure 4.7 Response of the sensor to 2 nd Piezoelectric Actuator Patch Group in Time Domain.....	43
Figure 4.8 FRF between the 2 nd Piezoelectric Actuator Patch Group and the Sensor	44
Figure 4.9 FRF for the 2 nd Piezoelectric Patch Group obtained by Mathematical Model and Experimental Data	44
Figure 4.10 Response of the sensor to 3 rd Piezoelectric Actuator Patch Group in Time Domain.....	45
Figure 4.11 FRF between the 3 rd Piezoelectric Actuator Patch Group and the Sensor	46
Figure 4.12 FRF for the 3 rd Piezoelectric Patch Group obtained by Mathematical Model and Experimental Data	47
Figure 5.1 Block Diagram of State Feedback Control System	50

Figure 5.2 Block Diagram of the Controlled System with State Observer	52
Figure 5.3 Bode Diagram of the Band Pass Filter for 1 st Controller Group	54
Figure 5.4 Bode Diagram of the Band Pass Filter for 2 nd Controller Group.....	54
Figure 5.5 Bode Diagram of the Band Pass Filter for 3 rd Controller Group	55
Figure 5.6 FRF for the Disturbance Patch obtained by Mathematical Model and Experimental Data.....	57
Figure 5.7 Plant Model.....	57
Figure 5.8 System Simulation	58
Figure 5.9 Active Vibration Control of the Plate due to an Initial Condition.....	59
Figure 5.10 Active Vibration Control of the Plate due to an External Force at the 1 st Natural Frequency	60
Figure 5.11 Controller Output to Suppress Vibration at the 1 st Mode	60
Figure 5.12 Active Vibration Control of the Plate due to an External Force at the 2 nd Natural Frequency	61
Figure 5.13 Controller Output to Suppress Vibration at the 2 nd Mode	61
Figure 5.14 Active Vibration Control of the Plate due to an External Force at the 3 rd Natural Frequency.....	62
Figure 5.15 Controller Output to Suppress Vibration at the 3 rd Mode.....	62
Figure 5.16 Simulated Controller Performances in Frequency Domain	63
Figure 5.17 Active Vibration Control of the Plate due to an Initial Condition.....	64
Figure 5.18 Active Vibration Control of the Plate due to an External Force at the 1 st Resonance Frequency.....	66
Figure 5.19 Controller Output to Suppress the 1 st Mode Vibration.....	66
Figure 5.20 Active Vibration Control of the Plate due to an External Force at the 2 nd Resonance Frequency	67
Figure 5.21 Controller Output to Suppress the 2 nd Mode Vibration	67
Figure 5.22 Active Vibration Control of the Plate due to an External Force at the 3 rd Resonance Frequency	68
Figure 5.23 Controller Output to Suppress the 3 rd Mode Vibration.....	68
Figure 5.24 Attenuation of the 1 st mode via each Controller Groups	69

Figure 5.25 Attenuation of the 2 nd mode via each Controller Groups	69
Figure 5.26 Attenuation of the 3 rd mode via each Controller Groups.....	70
Figure 5.27 Attenuation of the 1 st mode via 1 st and all Controller Groups.....	71
Figure 5.28 Attenuation of the 2 nd mode via 2 nd and all Controller Groups	71
Figure 5.29 Attenuation of the 3 rd mode via 3 rd and all Controller Groups.....	72
Figure 5.30 Comparison of the System Response of the 1 st Mode with and without Controller Group 1	73
Figure 5.31 Comparison of the System Response of the 2 nd Mode with and without Controller Group 2	73
Figure 5.32 Comparison of the System Response of the 3 rd Mode with and without Controller Group 3	74
Figure 5.33 Comparison of the System Responses with and without all Controllers	74

CHAPTER 1

INTRODUCTION

Lightweight structures become a must in aerospace engineering applications. In order to reduce the weight of the composite materials more, composite lamina are combined with lightweight core to introduce sandwich structures. Sandwich structures are beneficial due to having high strength and stiffness properties, long fatigue life resistance and smoother surface [1]. Although they are very advantageous over other engineering structures, various vibration problems may come into picture during their service life. In airframe design, vibro-acoustic coupling is considered as an important design restriction which may cause damage in the aircraft [2]. On the other hand, structures made of lightweight materials have low natural frequencies which may cause high amplitude oscillation problems. Newly designed lightweight robot manipulators are also in the field of interest of aerospace engineering. Nevertheless, due to the flexibility of the manipulator, vibration problems may cause performance loss of precision in positioning [3]. Another problematic issue related to vibration is the buildings since they are vulnerable to natural disasters such as earthquakes or high velocity winds as well as human-made calamities [4]. Furthermore, in space applications such as antennas or solar panels, instability and fatigue problems may occur due to vibrations as well [5].

In order to overcome those problems, some techniques are proposed. First, inserting passive materials such as masses, dampers or springs for passive vibration control may be considered. When passive vibration control techniques are not enough for vibration suppression, active vibration control techniques may come into consideration. Active vibration control is a very wide topic that a lot of people are working on it. Dubay et al. designed a predictive control for one-link flexible manipulator based on finite element model [6]. Li et al. proposed a PID controller for

noise control of vibro-acoustic system [2]. Halim et al. designed a controller for multi-link flexible robotic manipulator and performed a case study for a two-link robotic manipulator [3]. Dafang et al. experimentally showed that independent modal space control method can control each of the first three mode individually. In their specimen they attached separate piezoelectric patch groups to control each of the modes [7]. Additionally, Kerboua et al. controlled their beam via smart materials [8]. In their work, Zippo et al. are controlled a composite sandwich plate with honeycomb core through active vibration control [9].

Actuation force plays a significant role in active vibration control. In their work, Chevva et al. tried to use minimum actuation power in active vibration control [10]. On the other hand, Luo et al. studied active vibration control of sandwich panel with multi-layered piezoelectric actuator. They also took into consideration the physical parameters of the actuator on the actuation capability [11], [12]. Furthermore, Song et al. found optimum places of piezoelectric patches for supersonic flutter control of composite laminated panels [13]. Apart from these, active vibration control of sandwich beams and plates are studied [14]–[17]. Additionally, Ferrari et al. worked on sandwich plate active vibration control by non-collocated positive position feedback [18]. Subsequently, Active Vibration Control is implemented to a full scale space vehicle structure [19].

1.1 Background of the Study

In this section, a brief introduction for definitions is presented. First, sandwich materials are defined and some background information is given. After that, piezoelectric materials and their usage in active vibration control are mentioned. Furthermore, some basic information about active vibration control is given to illustrate the topic more understandable.

1.1.1 Sandwich Structures

Sandwich structures are simply constructed by placing a core between two skins which are thinner than the core. However, a formal definition says that a special form of different composite materials that are bonded to utilise the properties of each component for structural advantage [20], [21]. Sandwich structures are used in aerospace industries not only due to their low weight but also their high stiffness and strength properties. The skins of a sandwich structure are made of composites fibers or sometimes metals such as aluminium which have high stiffness and the core materials are selected as balsa, foam or honeycomb for their lightweight. According to their work, Hexcel Composites states that, with a honeycomb core as thick as the skins the relative stiffness of whole structure goes up seven times although the structure gains weight only 3%. A comparison is given in Table 1.1 [22].

Table 1.1 Honeycomb Sandwich Panel Structural Efficiency [22]

Property	Only Skin Material	Sandwich Structure with Core as thick as skin	Sandwich Structure with Core 3 times thicker than skin
Relative Stiffness	100	700	3700
Relative Strength	100	350	925
Relative Weight	100	103	106

The advantage of the sandwich structure can easily be observed through Table 1.1. An additional advantage of sandwich construction can be said as a sandwich structure does not have unique elastic properties but is designed to have desired properties [1]. Having all these advantages, sandwich structures are frequently used in aerospace industries as used in other engineering areas.

1.1.2 Piezoelectric Materials

Piezoelectricity is first discovered by Curie brother in 1880 while experimenting on crystallography which is defined as a generation of electricity due to mechanical displacements [23]. Piezoelectric Materials are also able to create strain due to voltage difference which is called as inverse piezoelectricity. An illustration for piezoelectricity is given in Figure 1.1 [24]. Piezoelectricity usually appears in insulative materials. They can be splatted up into two major groups which are ceramics and crystals [25]. Some piezoelectric materials are natural and found in the nature in crystal forms such as quartz which has many commercial usages. However lots of piezoelectric materials are manmade ceramic materials e.g. lead-zirconate-titanate (PZT), lead-titanate (PbTiO_2), leadzirconate (PbZrO_3), and barium-titanate (BaTiO_3) [26].

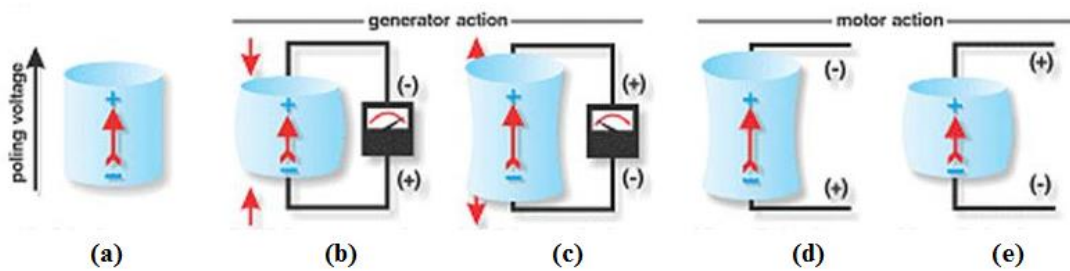


Figure 1.1 Generator and Motor Actions of a Piezoelectric Element: (a) disk after polarization, (b) disk compressed: generated voltage has same polarity as poling voltage, (c) disk stretched: generated voltage has polarity opposite that of poling voltage, (d) applied voltage has same polarity as poling voltage: disk lengthens, (e) applied voltage has polarity opposite that of poling [24]

Piezoelectric materials are produced by polarization methods. While arranging piezoelectric polymers, high poling electric field to the essentially insulating material is wanted [27]. Those piezoelectric materials have a great application area. For instance, electromechanical frequency filters, ultrasonic imaging, piezoelectric motors and transformers, piezoelectric positioning, injection systems, gyroscopes, pressure

and temperature sensors are some application areas for piezoelectric materials [27], [28].

1.1.3 Active Vibration Control

Main concept of the vibration cancellation is giving the balancing signal with a phase difference of 180° , which is anti-phase. In early applications, active noise control is studied, experimentally. Today, some headphones and microphones are suppressing the noise for a better listening. Furthermore, active vibration control is applied to ships [29] as well as are carried out in various marine applications [30]. Moreover, for more comfortable vehicles, controller techniques are used in automobile technologies [31]. Following those, active vibration control techniques are started to be applied on beams and plates having infinitely many degrees of freedom and different wave types propagating on them. These researches have a great influence in aircraft and spacecraft industry [32] including applications in helicopters. In fact, for gust reduction and wing flutter control, active vibration controllers have been specifically improved [33]. There are also other areas for active vibration suppression applications such as in civil engineering, optics, sound transmission and also in flow control [32].

Although there are other hardware for active vibration control, piezoelectric materials are very important and have a wide coverage in the industry. Because the piezoelectric materials are small and effective actuators as well as sensors, they are very common in controlling of lightweight structures. In addition, piezoelectric patches are available and cheap ceramics. Summing all those properties of active vibration control, sandwich structures and piezoelectric materials, in this thesis, active vibration control of sandwich structures via piezoelectric patches is studied.

1.2 Motivation of the Thesis

In the former researches conducted in the Department of Aerospace Engineering at Middle East Technical University, active vibration control of a smart beam and fin-like structures, made of isotropic material are studied [34]–[40]. In these studies, piezoelectric patches are attached to root section of the beam [41], [42]. For fin applications, piezoelectric patches are attached as actuators and the strain gages as sensors [43]. In this thesis, active vibration control of smart composite sandwich plate is examined, having the piezoelectric patches as sensors and actuators in their optimum locations. In fact, for each vibration mode of the sandwich plate, piezoelectric patches are located, and for each piezoelectric patch group separate controller is applied. After all of the controllers are operated, they are used together to suppress vibrations in first three modes of the plate.

1.3 Outline of the Thesis

The brief information about the coming sections of this thesis is given as follows:

In Chapter 2, Modal Analysis of the sandwich plate is performed. First, a finite element model is constructed. Then, the plate is tested via impact hammer and accelerometer to obtain its passive modal characteristics. Comparing the results of the finite element analysis results and the experimentally obtained ones, the finite element model is then updated.

In Chapter 3, locations for piezoelectric patches are found. First, the finite element model constructed in Chapter 2 is used to find the curvature of each mode shapes. Then, the sensor is located at the place where the combination of the curvatures of all mode shapes of interest is the maximum. After that, using same procedure, the disturbance actuator is located to be able to disturb the plate in its first three modes. Finally, the location algorithm is run to find the optimum locations of the actuator groups.

Chapter 4 presents the system identification and in this chapter, experimental setup is introduced. Using this experimental setup, data in time domain representing the characteristics of the system is obtained. After that, system matrices for each of the piezoelectric patch groups located according to the results obtained in Chapter 3 are obtained. Through the identification procedure, Fast Fourier Transform (FFT) is used for experimental data and the system matrices whose bode plots are close to the FFT results are determined.

In Chapter 5, active vibration control of the sandwich plate is performed. First, a pole placement controller is designed for the system. In order to work with the pole placement type controller, states of the system is needed to be known. To estimate the states of the system, a state observer is designed. Having completed the design of an observer, case studies are performed via experimental setup. All analyses results are also verified in this chapter.

In Chapter 6, the results of the research study are discussed and the future work is recommended.

CHAPTER 2

MODAL ANALYSIS OF THE SANDWICH PLATE

2.1 Introduction

In this chapter, modal analysis of the sandwich plate is performed. First, finite element model (FEM) is generated and modal analysis is performed to obtain the natural frequencies and the corresponding mode shapes. After that, in order to compensate the differences between the model and the real structure, experimental modal analysis is performed. The differences are tried to be minimized changing the material properties. At the end of this chapter, final model of the sandwich plate is constructed.

2.2 Finite Element Modelling and Analysis of the Sandwich Plate

A composite sandwich plate with the dimensions of 195 mm and 300 mm is modelled by using MSC Patran [44] finite element modelling tool and MSC Nastran [45] finite element solver. The plate has three layers such that the skin material is SGL GE8903-280-37e Prepreg E-glass and the core material is Rohacell 31 IG-F foam. The skins of the plate are produced having one layer of 0.25 mm thickness, each using glass fibers in twill weave form, and the core is 1 mm of foam. According to the material properties supplied from the manufacturer, the skins are assumed to be 2D orthotropic whereas the core of the plate is modelled as isotropic. The material properties are given in Table 2.1 and Table 2.2 respectively. For the skin, a range is given; and therefore the mean values are used.

Table 2.1 Material Properties of SGL GE8903-280-37e Prepreg E-Glass

	E₁	E₂	G₁₂	ρ
	[GPa]	[GPa]	[GPa]	[kg/m³]
Range	22.0 – 28.0	22.0 – 28.0	3.0 – 4.0	1900 - 2100
Used Value	25.0	25.0	3.5	2000

Table 2.2 Material Properties of Rohacell 31 IG-F Foam

E	G	ρ
[MPa]	[MPa]	[kg/m³]
36.0	13.0	32

In Table 2.1, E_1 and E_2 are for the Young's modulus values in two perpendicular fiber directions of the skin material, respectively. Since the material has fibers in both directions, Young's modulus values are equal in both directions. G_{12} is for shear modulus of the skin material, and ρ is the density. In Table 2.2, since the core material is assumed to be isotropic, E , G , ρ is for Young's modulus, shear modulus and density, respectively.

The plate is modelled as composite with three layers comprising an isotropic core in between two 2-D orthotropic skins in each side. The whole structure is modelled with CQUAD4 2-D shell elements using MSC Patran Software. Different mesh densities are performed to show that the results are independent of the mesh assigned. As it can be seen from Figure 2.1, 8 elements for the short edge and 12 elements for the long edge is enough for the mesh independency of the first three natural frequencies which are corresponding to the first out-of-plane bending, the first torsional and the second out-of-plane bending modes.

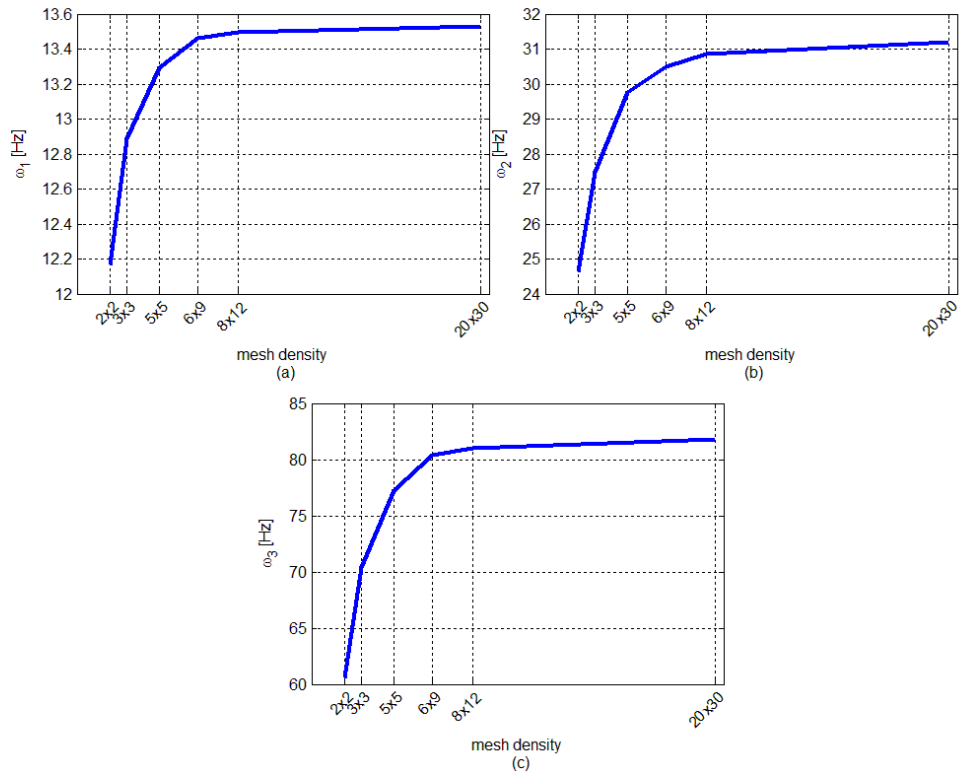


Figure 2.1 Mesh Convergence Plots (a) 1st Natural Frequency, (b) 2nd Natural Frequency, (c) 3rd Natural Frequency

Another decision mechanism for the mesh density will come into picture while locating the piezoelectric patches. In order to find the precise locations for the patches it is required to have 60 elements along the short edges and 90 elements along the long edges. Since 60 by 90 elements do not cause mesh dependency, that density for mesh is decided to be used. Therefore the finite element model includes 5400 elements and 5551 grid points. The natural frequencies and the corresponding mode shapes obtained from the finite element analysis (FEA) are given in Figure 2.2.

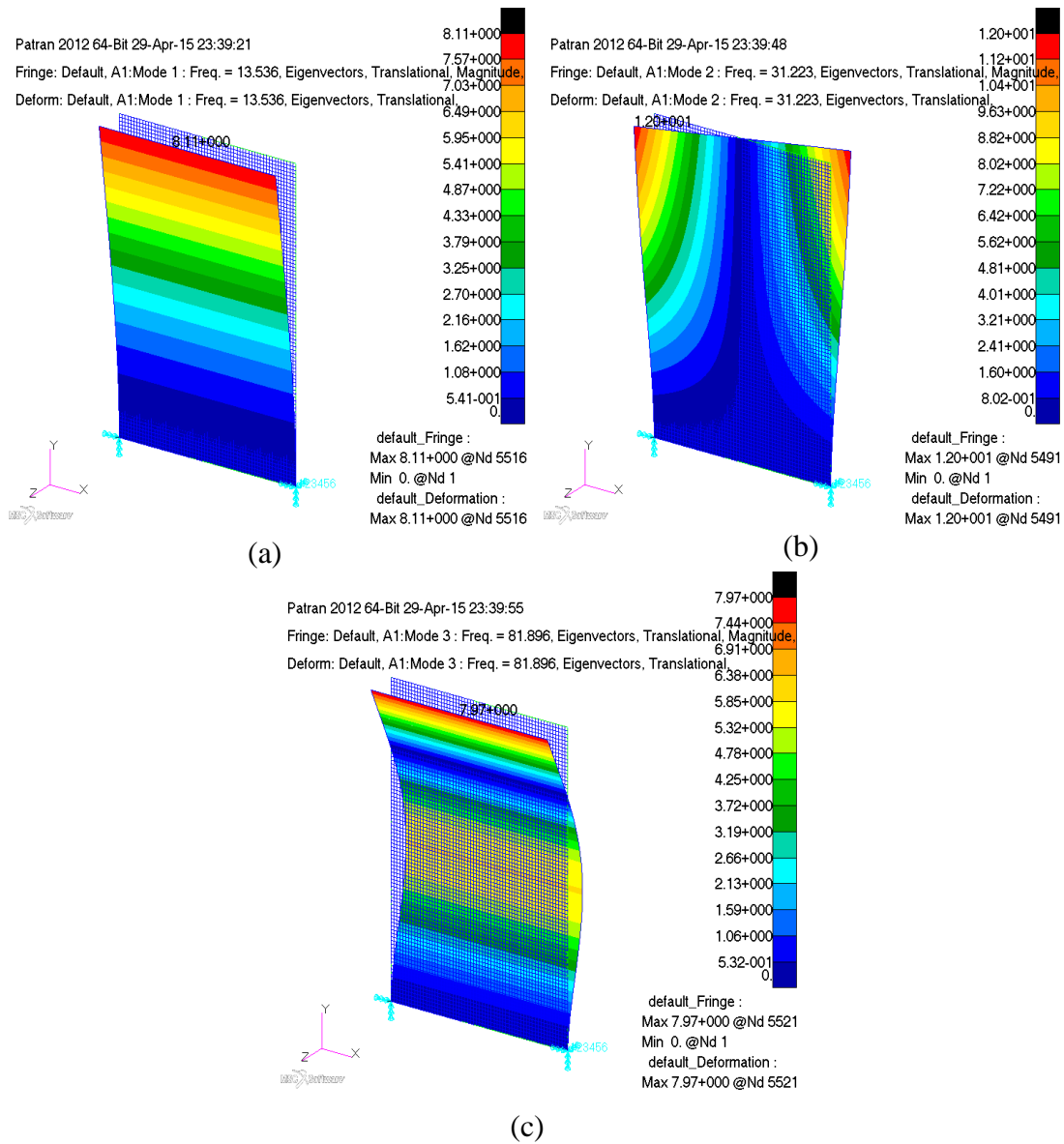


Figure 2.2 Natural Frequencies and the Corresponding Mode Shapes of the Sandwich Plate by FEA: (a) First Out-of-Plane Bending Mode [13.54 Hz], (b) First Torsional Mode [31.22 Hz], (c) Second Out-of-Plane Bending Mode [81.90 Hz]

2.3 Experimental Modal Analysis (EMA) of the Sandwich Plate

So as to verify the FEM, a modal test for the sandwich plate is performed with a B&K 4517-002 Single Axis Accelerometer [46] of 1 gram (Figure 2.3 - c) and B&K 8206 Impact Hammer [46] with an aluminium tip (Figure 2.3 - b) through B&K

software and hardware [47] which is a 6-Channel PULSE Data Acquisition System (Figure 2.3 - a). The accelerometer is attached to the specimen with a thin layer of bee wax. Note that, the aluminium tip for the impact hammer can excite the structure up to 1 kHz [47].

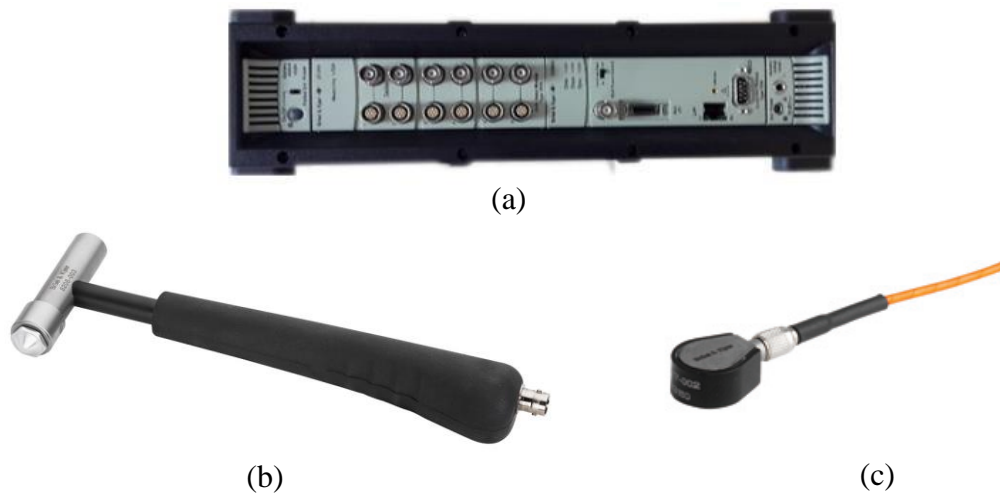


Figure 2.3 Modal Analysis Test Equipment [47]: (a) B&K 6-Channel PULSE Data Acquisition System, (b) B&K 8206 Impact Hammer, (c) B&K 4517-002 Single Axis Accelerometer [46]

First of all, one of the short edges of the specimen with the dimensions of 195 mm and 300 mm is clamped to create a fixed boundary condition as shown in Figure 2.4. The coordinate system shown in Figure 2.4 is used as the global coordinate system throughout this thesis.

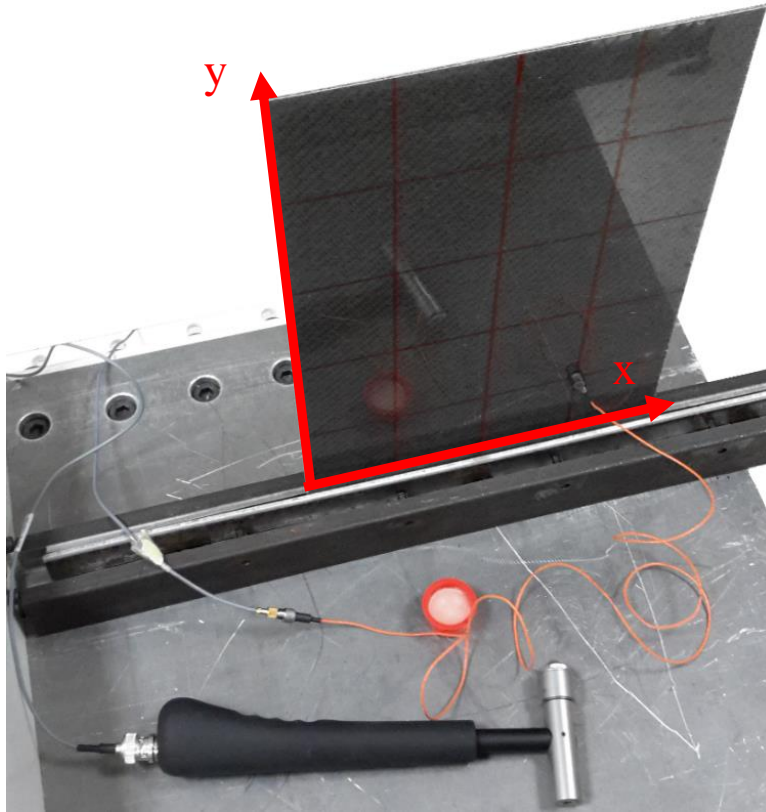


Figure 2.4 Modal Analysis Test Setup (Oblique View)

To perform a modal test, 30 points are determined on the specimen and the measurements are taken from 25 points as a single-input single-output (SISO) system. The first five points along the short edge are assumed to have zero displacement since they are at the fixed boundary and no measurement is taken on them. The accelerometer (shown with a red arrow) is attached to point 9 and from point 6 to point 30 the impact hammer (shown with a hammer) is roved as it can be seen from Figure 2.5.

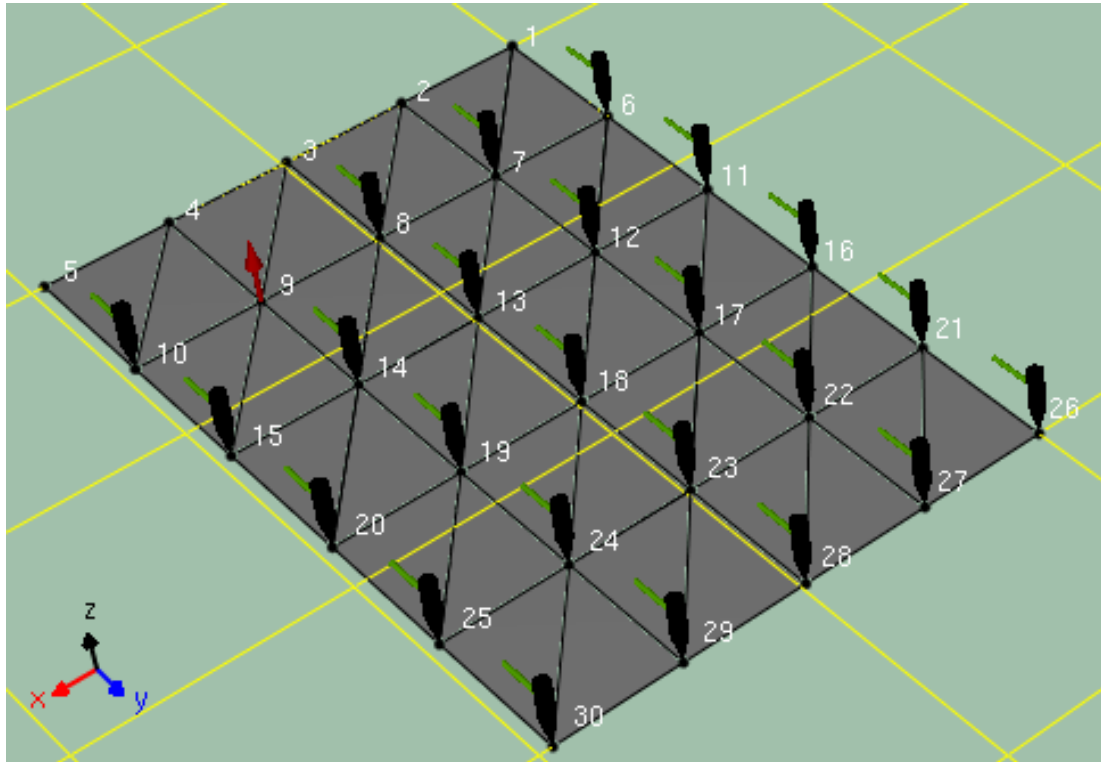


Figure 2.5 Test Points on the Specimen

In the experiment, 25 points are hit and the response from the accelerometer is measured. After the Fast Fourier Transform (FFT) analysis is completed the Accelerance Frequency Response Functions (FRFs) are obtained. For FFT analysis, 200 Hz frequency span is divided into 1600 lines and therefore the frequency resolution becomes 0.125 Hz. 10 hit for each point is averaged linearly by rejecting the overloads for the accelerometer. Having completed all the measurements, the first three resonance frequencies are found by using the Reflex Modal Analysis Software [47]. Through this software, stability diagram is plotted using Polyreference Frequency Method for parameter estimation between the range from 5 to 100 Hz and the resonance frequencies are selected according to the least complexity. Stability Diagram for Point FRF is shown in Figure 2.6. According to the stability diagram, resonance frequencies and the corresponding mode shapes are obtained and presented in Figure 2.7.

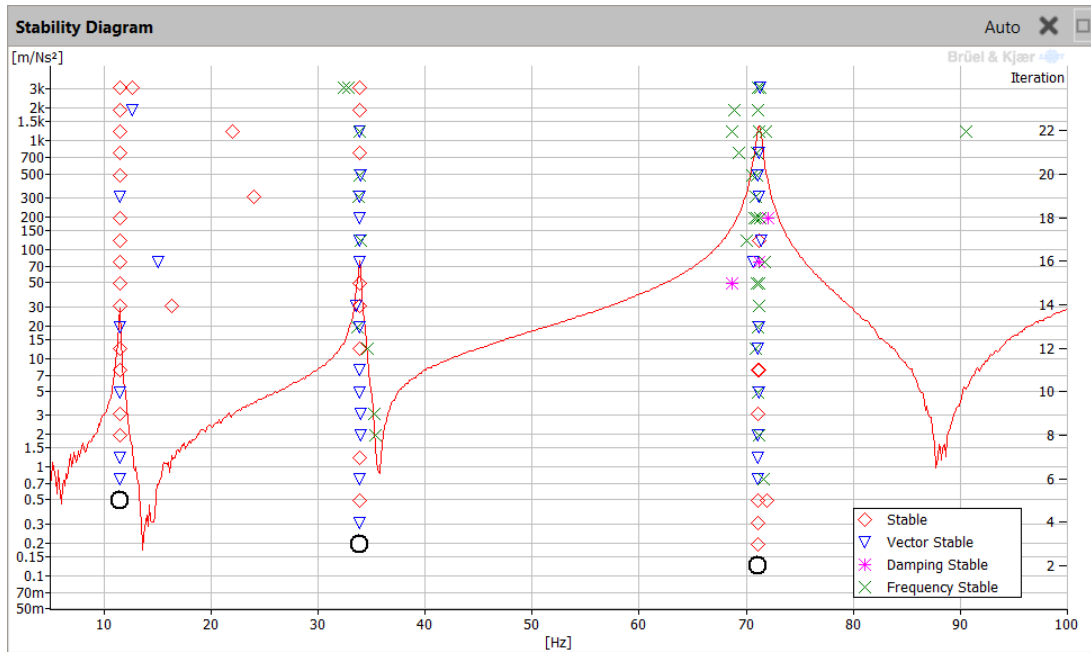


Figure 2.6 Stability Diagram of Point FRF

Tabulated results for the EMA and their comparison with the FEA can be shown in Table 2.3. As there is a difference between the results obtained by FEA and that of by the experiment, the model used in FEA is updated. Note that the percentage difference for each mode shape is calculated by Equation (2.1) and ω is used for the resonance and/or natural frequency.

$$Difference = \left| \frac{\omega_{EMA} - \omega_{FEA}}{\omega_{EMA}} \right| \times 100 \quad (2.1)$$

Table 2.3 Natural and Resonance Frequencies of the Sandwich Plate

	ω_1 [Hz]	ω_2 [Hz]	ω_3 [Hz]
FEA	13.54	31.22	81.90
EMA	11.53	33.94	71.11
Difference %	17.43	8.01	15.17

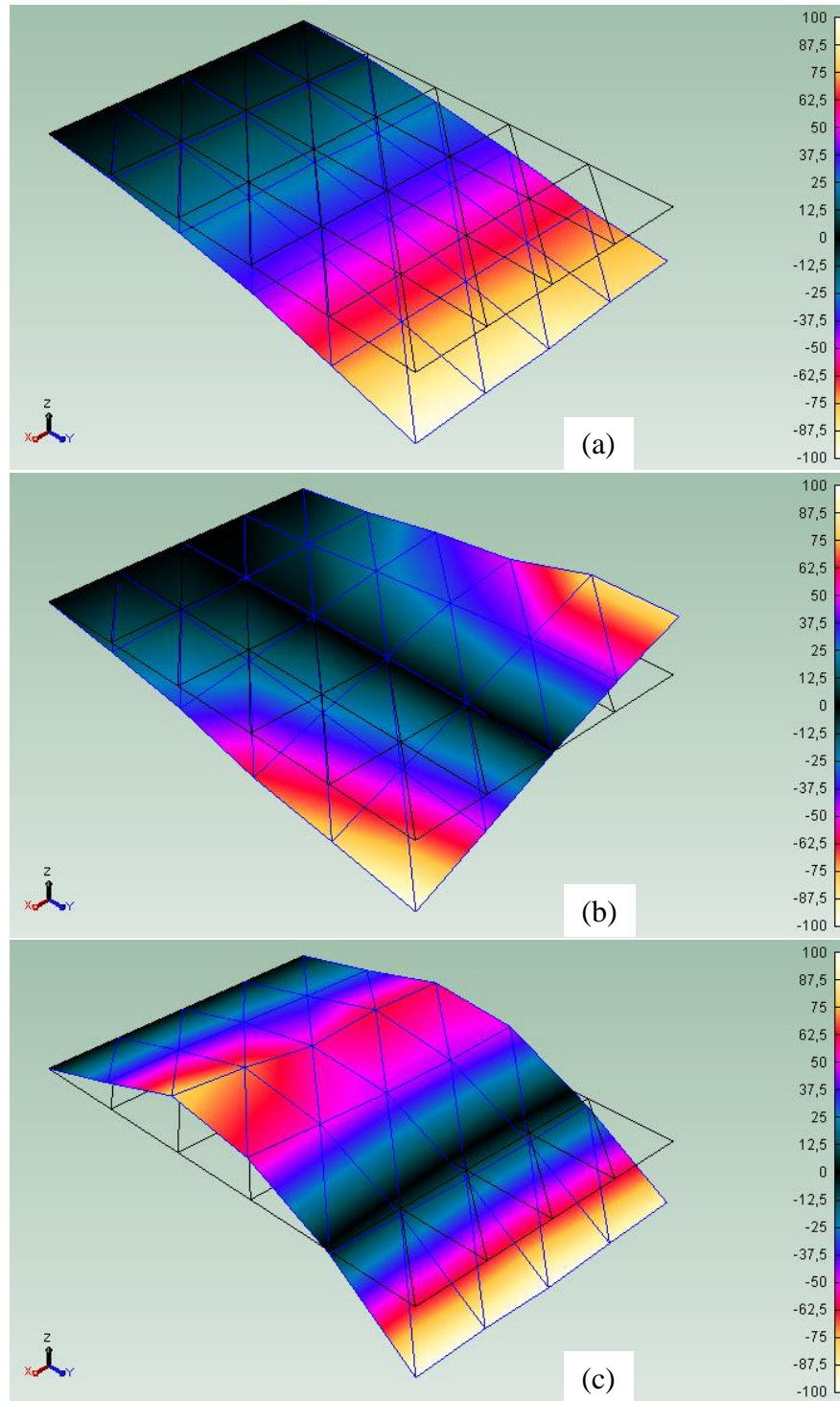


Figure 2.7 Resonance Frequencies and the corresponding Mode Shapes of the Sandwich Plate by EMA: (a) First out-of-Plane Bending Mode [11.53 Hz], (b) First Torsional Mode [33.94 Hz], (c) Second out-of-Plane Bending Mode [71.11 Hz]

2.4 FEM Updating based on EMA Results

After the comparison of the FEA and EMA results, the difference between the resonance and natural frequencies can be seen clearly from Table 2.3. In addition, a MAC (Modal Assurance Criterion) Matrix is constructed between the FEA and EMA results to show the relation between the first three mode shapes. Formulation of MAC matrix is given in Equation (2.2) [48].

$$MAC(r, q) = \frac{|\{\varphi_A\}_r^T \{\varphi_X\}_q|^2}{(\{\varphi_A\}_r^T \{\varphi_A\}_r)(\{\varphi_X\}_q^T \{\varphi_X\}_q)} \quad (2.2)$$

Where;

$\{\varphi_X\}_q$: modal vector from experiment for mode shape q

$\{\varphi_X\}_q^T$: transpose of $\{\varphi_X\}_q$

$\{\varphi_A\}_r$: compatible analytical modal vector, mode shape r

$\{\varphi_A\}_r^T$: transpose of $\{\varphi_A\}_r$

According to the MAC Matrix, diagonal terms are very close to 100% which means the correlation between each of the modes is acceptable as shown in Table 2.4. Additionally, the off-diagonal elements are very close to zero except (1, 3) and (3, 1) elements of the matrix. In order to have closer natural frequencies to the ones obtained from EMA and to have a better MAC Matrix, model updating is performed on the FEM of the sandwich plate. As the MAC matrix obtained before the update has already indicated a good correlation between the experimental and finite element analysis results, it is not expected to have a greater improvement regarding the system natural frequencies.

Table 2.4 MAC Matrix between FEA and EMA before Model Updating

		Experiment		
		1	2	3
FEM	1	99.229	0.257	9.553
	2	0.163	98.844	0.173
	3	12.629	0.069	98.173

Remember that, the material properties are given as a range and the central values of them were used in the analysis. It can be said that the elastic coefficients of the skin may be different than the central values. Having E_1 and E_2 are equal, an updating process is performed using the software so-called FEMtools [49]. Attention is paid to have the 2-D orthotropic elastic properties of the fiber glass skin are in the specified ranges given for each of them. The material properties of the core material is not updated and the resultant material properties for the skin is presented in Table 2.5. The final natural frequencies found by the new updated FEM compared with the previous and the experimentally obtained ones are given in Table 2.6. In addition to these, new MAC Matrix is also given in Table 2.7.

Table 2.5 Updated Material Properties of SGL GE8903-280-37e Prepreg E-Glass

	E_1	E_2	G_{12}	ρ
	[GPa]	[GPa]	[GPa]	[kg/m ³]
Used Value	22.0	22.0	4.0	2100

Table 2.6 Natural Frequencies found by EMA and FEA before and after the Updating

	ω_1 [Hz]	ω_2 [Hz]	ω_3 [Hz]
EMA	11.53	33.94	71.11
FEA (before)	13.54	31.22	81.90
Difference %	17.43	8.01	15.17
FEA (updated)	12.41	31.42	75.39
Difference %	7.63	7.42	6.02

Table 2.7 MAC Matrix between FEA and EMA after Model Updating

%		Experiment		
		1	2	3
FEM	1	99.228	0.252	9.576
	2	0.163	98.864	0.173
	3	12.653	0.073	98.160

After the model updating, it can easily be seen that the difference between the natural frequencies by FEA and the experimentally obtained ones has been dropped drastically as expected. On the other hand, it is observed that the difference between the MAC Matrices before and after the updating has not changed much. Finite Element Model is constructed with the material properties taken from the manufacturing company and according to these properties; the skin of the plate is modelled as 2-D orthotropic and the core as an isotropic one. The accuracy of the model depends on those modelling assumptions as well as the material properties. Throughout the update process, only material parameters are changed and for this reason, there is still a small difference between FEA and EMA results.

2.5 Conclusion

In this chapter, FEM of the sandwich plate is generated. After the modelling of the plate, an impact hammer test is applied and the experimental results are obtained. The FEA results are updated and more accurate FEM for the sandwich plate is obtained. In the next chapter, the obtained mode shapes will be used in the location selection for the actuator and sensor pairs (i.e. surface bonded PZT patches).

CHAPTER 3

DETERMINATION OF THE ACTUATOR AND SENSOR LOCATIONS FOR THE SANDWICH PLATE

3.1 Introduction

It is very common that piezoelectric materials as patches are used in active vibration control applications to suppress excessive vibrations on the host structure with some electrical energy. Although the more electrical energy suppresses the vibrations quicker, it has some physical limits. In 2-D plate-like structures, the locations of the piezoelectric patches affect the time of suppressions and attenuation levels at the same electricity level. In fact, some locations make the structure unobservable and uncontrollable [50].

There are several ways to determine the locations for piezoelectric patches. In a particular technical review, Gupta et al. state that, the location for the piezoelectric patches can be found by some of the optimization criteria, such as, maximization of deflection of the host structure, maximization of modal forces or moments applied by the actuator, minimal change in host structural dynamics, desired host structural dynamics, maximization of degree of controllability and observability of modes of interest and minimization of control effort or host vibrations [51].

Controllability and observability concepts depend on the system dynamics, the locations and the numbers of actuators and sensors, respectively. The locations of the least electrical energy consumed and the highest modal forces generated can be considered as an optimal locations for the actuators [51]. Additionally, for the sensors, locations of large changes in the mode shapes or corresponding to high vibration amplitudes are considered as the best locations [52].

In order to locate piezoelectric patches maximizing the modal forces and moments applied on the structure, one should find the locations of maximum curvature. Note that, the slope is the first spatial derivative of the displacement and the second special derivative of the displacement is the curvature of the structure which is also proportional with the measured strain. In order to find the maximum value of the curvature, it is convenient that the derivative of it should be equated to zero which is the third spatial derivative of the displacement mode shape as shown in equation (3.1) [53]. Note that, w represents the displacement mode shape, x and t are for the location and time, respectively.

$$\frac{\partial^3 w(x, t)}{\partial x^3} = 0 \quad (3.1)$$

Note that the sensor location is found by maximizing the applied sensor voltage [53]. Equation (3.1) can also be used for location optimization for both sensors and actuators and minimizing [51]. Since the criteria given in equation (3.1) is available for locating both sensors and actuators; in this work, it is used for determination of the locations of the both sensors and actuators.

Also note that, in this work, the structure to be controlled has two dimensions. Therefore, in the sandwich plate case, change in y -dimension should be considered in a similar fashion as in equation (3.1). Thus, equations (3.2) and (3.3) are used in this study to find the curvature of each mode shapes and the piezoelectric patches are located over the surface on the structure where the maximum curvature occurs.

$$curvature_{e_x \text{ direction}} = \frac{\partial^2 w(x, t)}{\partial x^2} \quad (3.2)$$

$$curvature_{e_y \text{ direction}} = \frac{\partial^2 w(y, t)}{\partial y^2} \quad (3.3)$$

3.2 Determination of the Location of the Piezoelectric Sensors

In this work, locations of the piezoelectric patches are determined by using equations (3.2) and (3.3). The designed locating algorithm is based on the finite difference formula for the second derivative of each mode shapes in both x and y directions. For the locating algorithm, finite difference forms of equations (3.2) and (3.3) are given in below equations (3.4) and (3.5).

$$\frac{\partial^2 w(x, t)}{\partial x^2} = \frac{w(x + dx) - w(x) + w(x - dx)}{dx^2} \quad (3.4)$$

$$\frac{\partial^2 w(y, t)}{\partial y^2} = \frac{w(y + dy) - w(y) + w(y - dy)}{dy^2} \quad (3.5)$$

In the equation dx represents the difference between locations of each grid points. This formula is used to find the curvatures of the mode shapes of the updated FEM found in Section 2.4. The mode shapes are imported from the output of the finite element software MSC Patran and MSC Nastran. After that, the curvatures are calculated by using equations (3.4) and (3.5). The mode shapes and the corresponding curvatures in both x and y directions are shown in Figure 3.1, Figure 3.2 and Figure 3.3. Note that, the curvature calculated in x-direction is too small compared to the curvature in y-direction. Therefore, the maximum values of the curvatures for each mode are normalized to one for better presentation. In fact, the maximum values of the mode shapes are also normalized to one.

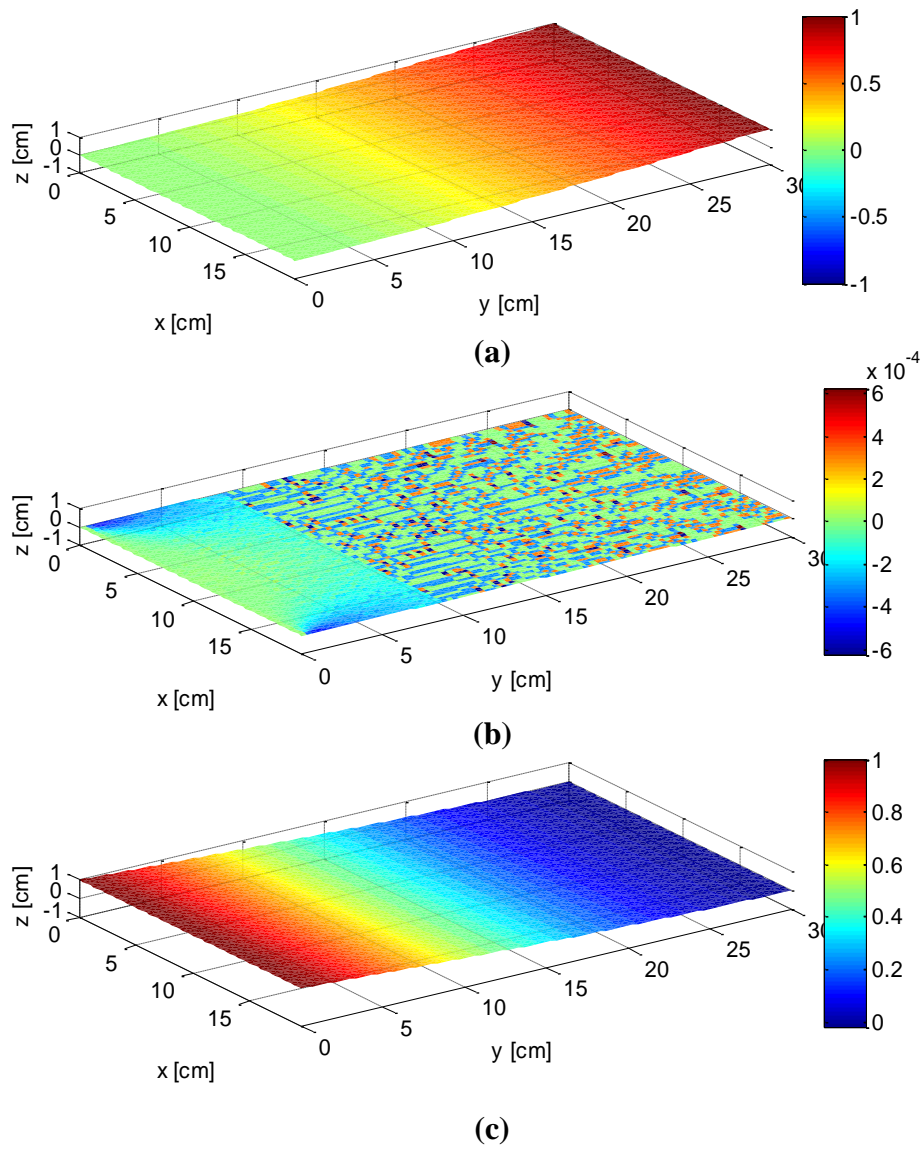


Figure 3.1 Sandwich Plate: (a) 1st Mode Shape, (b) Curvature in x direction, (c) Curvature in y direction

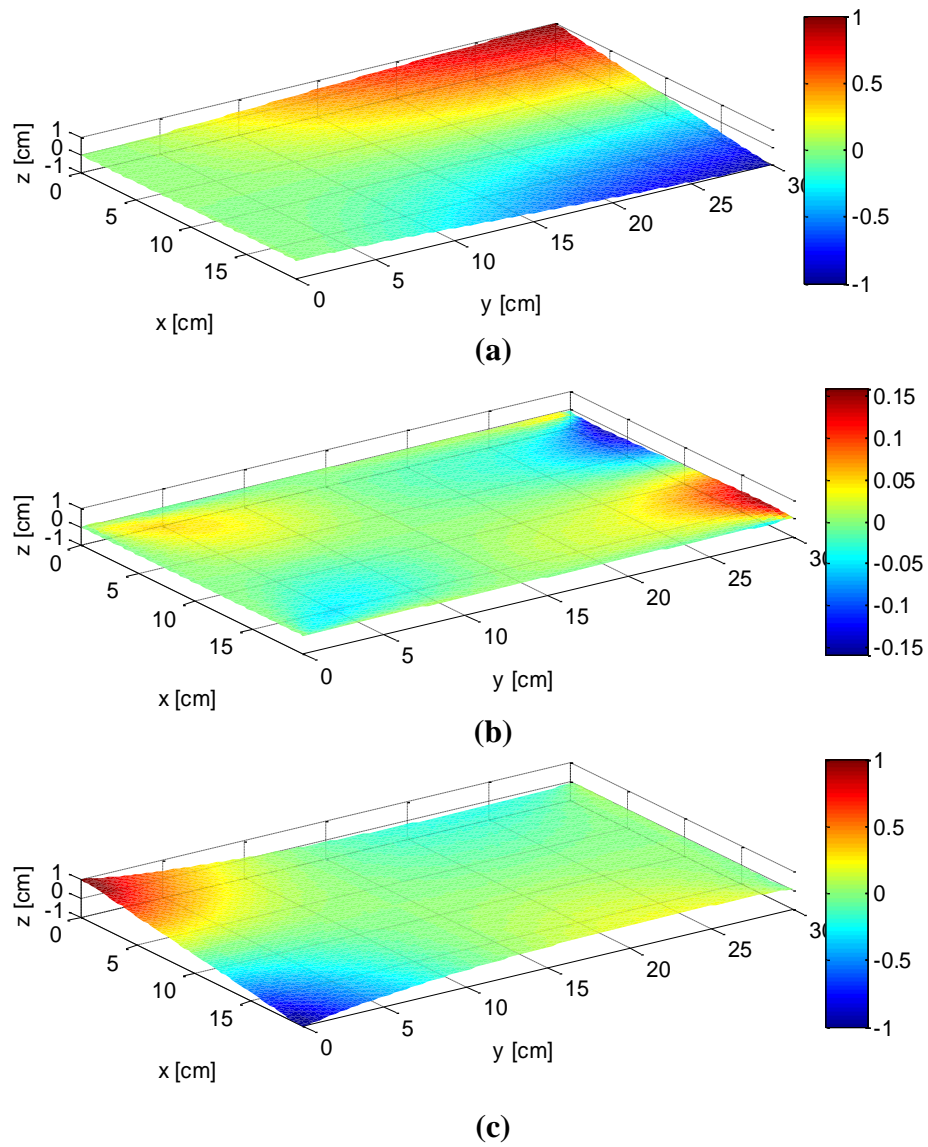


Figure 3.2 Sandwich Plate: (a) 2nd Mode Shape, (b) Curvature in x direction, (c) Curvature in y direction

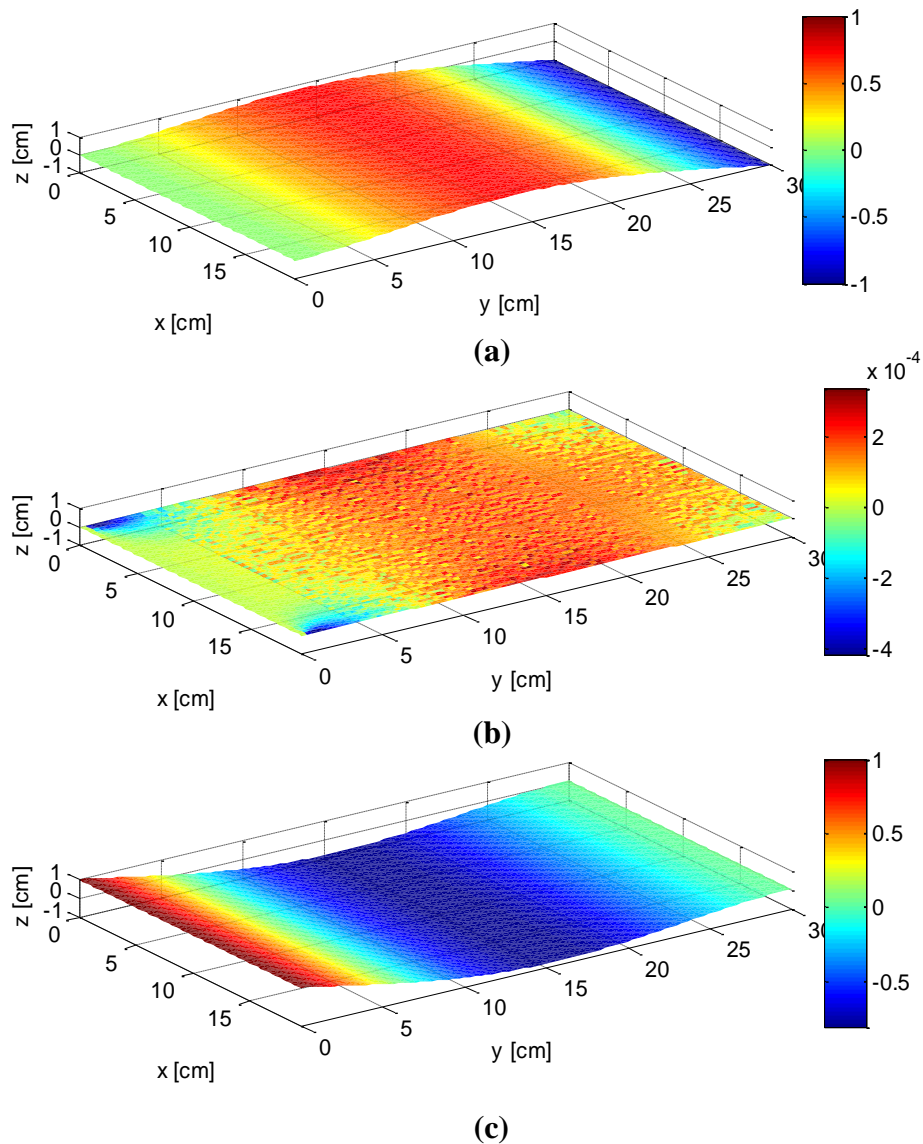


Figure 3.3 Sandwich Plate: (a) 3rd Mode Shape, (b) Curvature in x direction, (c) Curvature in y direction

As it can easily be seen from the figures, the maximum curvatures in y direction of all modes are in the root of the plate. Since, curvatures in x-direction are too small compared to the ones in y-direction, it is clear that the only sensor will take place in the root. In fact, looking at the 1st and 3rd modes, the curvatures are the highest at the whole root section but considering the 2nd mode, maximum curvature values are at the

corners of the root. This phenomenon implies that the only sensor will be located at one of the corners near the root of the plate structure.

Note that, the size of the piezoelectric patches are another input for the location design. In this work, SensorTech - BM500 piezoelectric (PZT, Lead - Zirconate - Titanate) patches (25 x 25 x 0.5 mm) are used [54]. The piezoelectric patch can be seen in Figure 3.4.



Figure 3.4 Piezoelectric Patch (SensorTech - BM500 PZT Patch)

The locating algorithm is working based on the curvatures in both directions. It adds the values and finds the location for the sensor. Since the system is symmetrical, there are two locations for the sensor; nevertheless, the algorithm selects the points which has a smaller grid number because there is no physical difference. The resultant location for the sensor is shown in Figure 3.5. And, it can be said that the sandwich plate is now a “Sensory Sandwich Plate”.

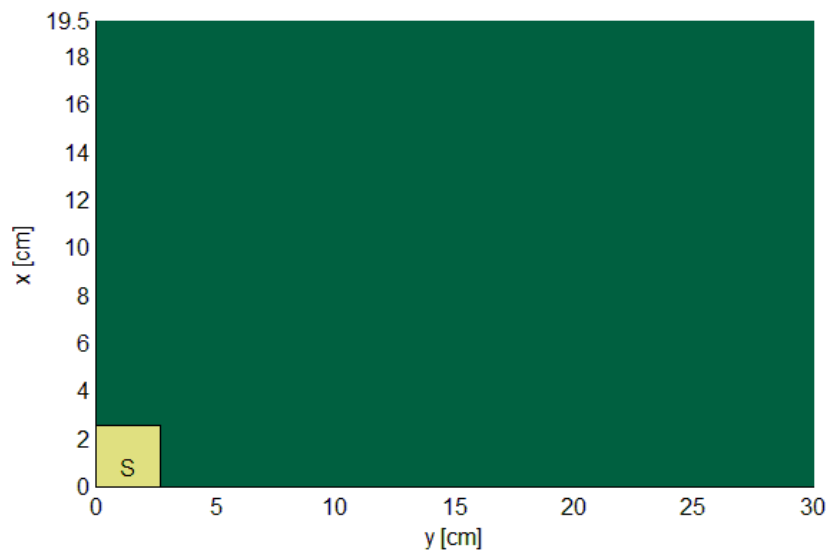


Figure 3.5 Location of the Piezoelectric Patch as a Sensor

3.3 Determination of the Locations of the Piezoelectric Actuators

Locations for the piezoelectric actuators will be found by following the same approach introduced in the previous section. Nonetheless, a piezoelectric patch has already been placed on plate which makes a new constraint for the placement procedure. While locating the sensor, the whole plate was available. On the contrary, actuators are located considering the places which already been filled and those places should not be selected and patched again.

The proposed placement algorithm works as follows;

1. $n=1$ (i.e. mode shape number)
2. Get the amount of the piezoelectric patches for each mode shape as input.
3. Find the curvature of the mode shape $\#n$.
4. Locate the piezoelectric patch to the maximum curvature location.
5. Deduct the value of the patched grids to zero.
6. Repeat steps 4 and 5 until all the patches for the corresponding mode shape are attached to the plate.
7. Increase number n by 1.
8. Stop if the number n is greater than the number of the interested modes else go through the steps 3 to 7.

Flowchart representation of the algorithm is given in Figure 3.6.

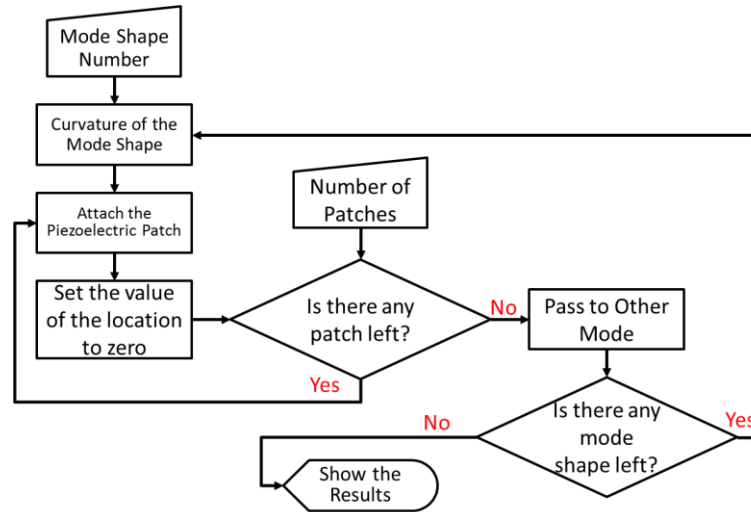


Figure 3.6 Flowchart of the Placement Algorithm

The number of the piezoelectric patches are selected iteratively, considering the following physical constraints of the plate. First, the location of the sensor is selected and introduced as a restriction for actuator placements. Secondly, since a disturbance patch is needed for the experimental purposes (i.e. forced vibration suppression), it is placed and also introduced to be a restriction for actuator placements as well. Disturbance patch is also selected as a PZT patch which is used to supply disturbance signals to the system in the experimental cases. So as to provide a symmetry, the disturbance PZT patch location is chosen to be the corner of the plate. Plate with the sensor (S) and the disturbance (D) patches is shown in Figure 3.7. Then, for the first mode, 4 piezoelectric patches are added. Since 6 patches can be attached to a line in x-direction and the maximum curvature for the first mode occurs at the root of the plate, 1 sensor, 1 disturbance and 4 controller actuators are decided. After that, 4 patches for the second and the third modes are selected. For each mode, the curvature is calculated excluding the locations which already have some patches. The locations of the piezoelectric actuators are given in Figure 3.8. In the figure, red squares represent the patches for the first mode, the green ones for the second mode and the blue ones are for the third mode. In fact, the piezoelectric patch groups are called with their mode number. They are also numbered as 1 to 4 for the 1st, 5 to 8 for the 2nd and 9 to 12 for the 3rd mode and these numbers are given to the patches according to their

placement order. The all piezoelectric patches located on the sandwich plate including both sensor and actuators are given in Figure 3.9.

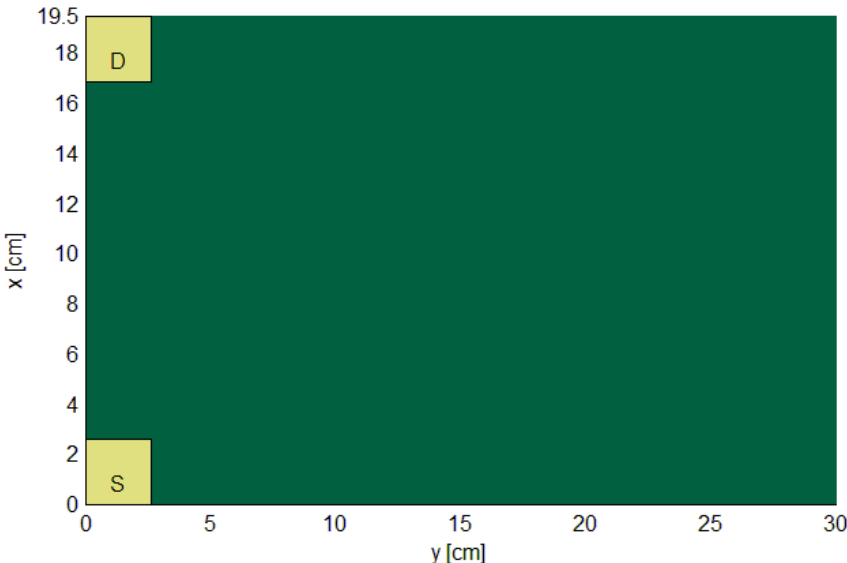


Figure 3.7 Locations of the Piezoelectric Patches for Disturbance and Sensor

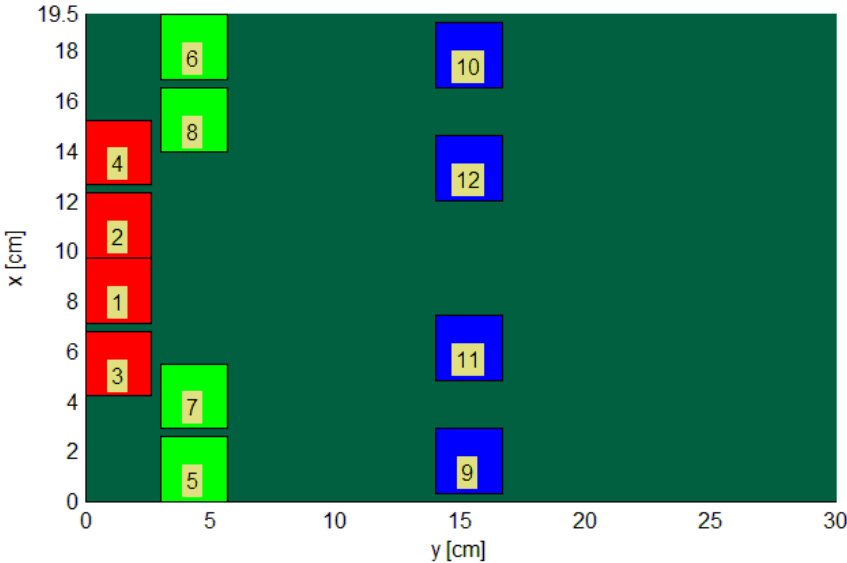


Figure 3.8 Locations of the Piezoelectric Actuators

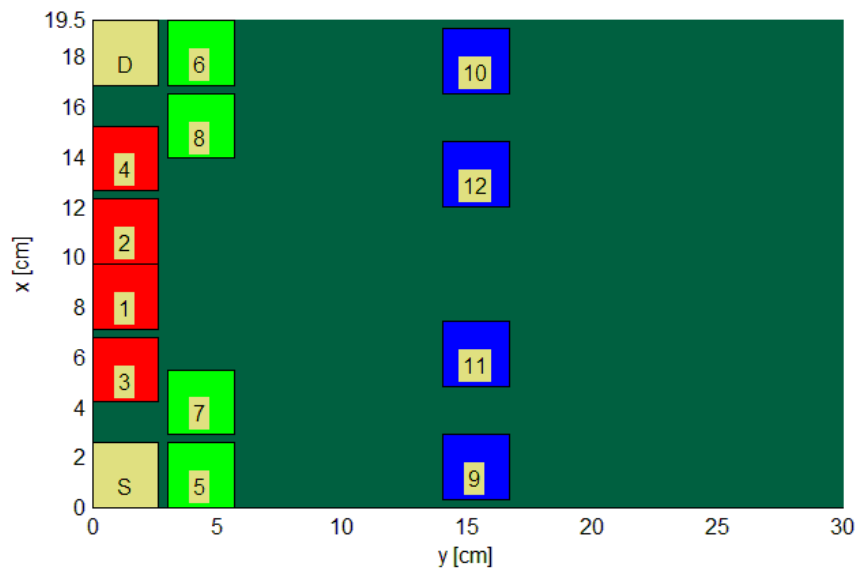


Figure 3.9 Locations of all Piezoelectric Patches

Piezoelectric patches are attached to the structure using ‘Bison 2-component epoxy adhesive’ [55]. According to the results represented in Figure 3.9, some of the piezoelectric patch locations are difficult to be placed exactly at the locations found by the algorithm as they should not touch each other. Therefore, by considering this issue as well, the final patch locations are shown in Figure 3.10.

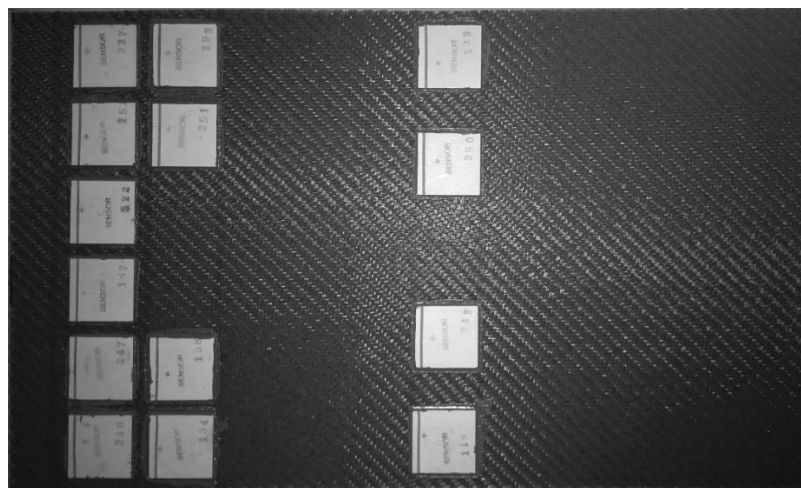


Figure 3.10 Smart Sandwich Plate

3.4 Conclusion

In this chapter, locations of the piezoelectric patches are determined by considering the curvature of the each mode of interest. First, the location of the PZT sensor patch is determined. After that, the disturbance PZT patch to be controlled is placed. Finally, all the controller patches are located over the surface of the plate. From now on, sandwich plate with sensors and actuators will be called as “Smart Sandwich Plate”.

CHAPTER 4

SYSTEM IDENTIFICATION OF THE SMART SANDWICH PLATE

4.1 Introduction

System characteristics are very important in order to design any kind of controller. Before checking the controller performance experimentally, the system model is needed to be simulated. According to the simulation results, controller may be tuned or even the controller of structure may be changed. On the other hand, in controller design, system matrices are used for both controller coefficients and in the observer design. In this section, how the system model is derived is explained in details. First of all, the experimental setup is introduced and the procedure is stated. A sine chirp signal with a frequency interval of which is in between 1 and 100 Hz is applied separately from each of the actuators. The interval is selected based on the finite element model constructed in Chapter 2 to cover the first three modes of the plate. While the chirp is applied from each of the actuators, the piezoelectric sensor patch is used to record the time history due this chirp signal. Time domain data is then analysed by Fast Fourier Transform (FFT) to find frequency domain characteristics and to construct a mathematical model of the system in Laplace domain.

4.2 Experimental Setup

Smart Sandwich Plate in Figure 4.1 is a cantilevered composite sandwich plate with 14 surface bonded SensorTech - BM500 piezoelectric (PZT, Lead - Zirconate - Titanate) patches of size 25 x 25 x 0.5 mm.

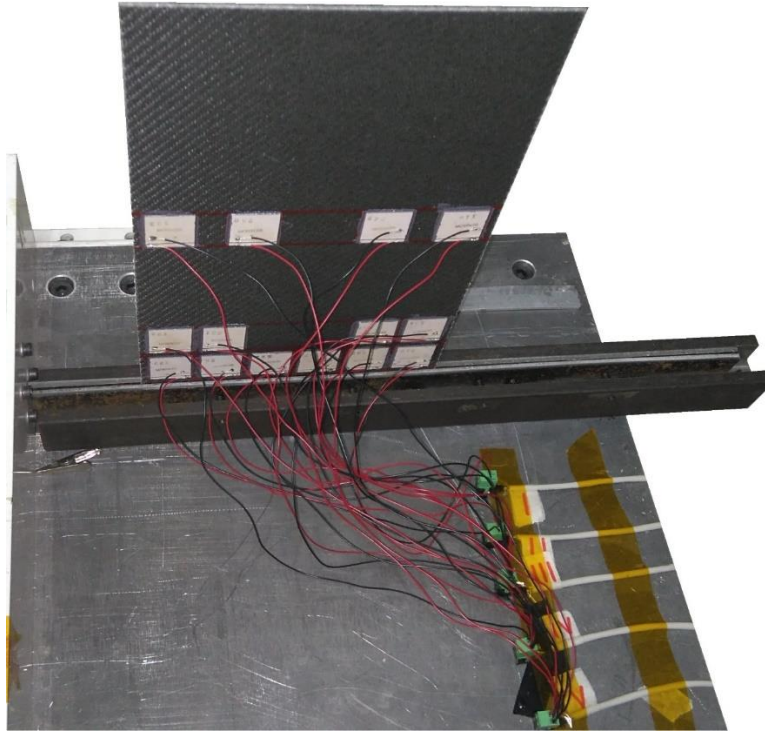


Figure 4.1 Smart Sandwich Plate

Each piezoelectric patch group are excited with SpeedGoat Real Time Target Machine [56] which can produce $\pm 10\text{V}$ peak-to-peak signal. This signal can be amplified 30 times by SensorTech SA10 high voltage amplifier in Bridge mode [57] which is powered by a SensorTech SA21 High Voltage Power Supply. Nevertheless, SensorTech SA10 high voltage amplifier has an input voltage capacity of $\pm 9\text{V}$ maximum. Therefore the output obtained from the whole system for piezoelectric actuation is $\pm 270\text{V}$ at most. In the plots representing experimental results voltage sent from SpeedGoat Real Time Target Machine is shown for simplicity. Experimental setup configuration is shown schematically in Figure 4.2.

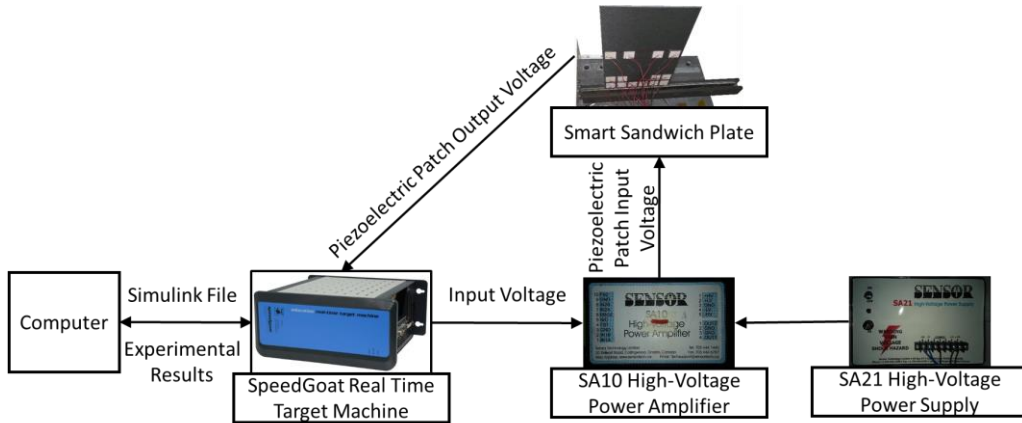


Figure 4.2 Experimental Setup Configuration

4.3 Mathematical Modelling of the Experimental System

The Frequency Response Functions (FRF) for each of the piezoelectric actuator groups are found by getting the ratio of the output signal obtained through the piezoelectric sensor to the input signal which is sent to each of the piezoelectric actuator groups. In order to have a clearer plot for FRF, a sine chirp with 150V peak-to-peak amplitude within a bandwidth 1-100 Hz is used as the input. The first 50 seconds time history of the input signal produced by SpeedGoat Real Time Target Machine before amplified by SA10 high voltage amplifier is shown in Figure 4.3 where the peak-to-peak amplitude is 5V.

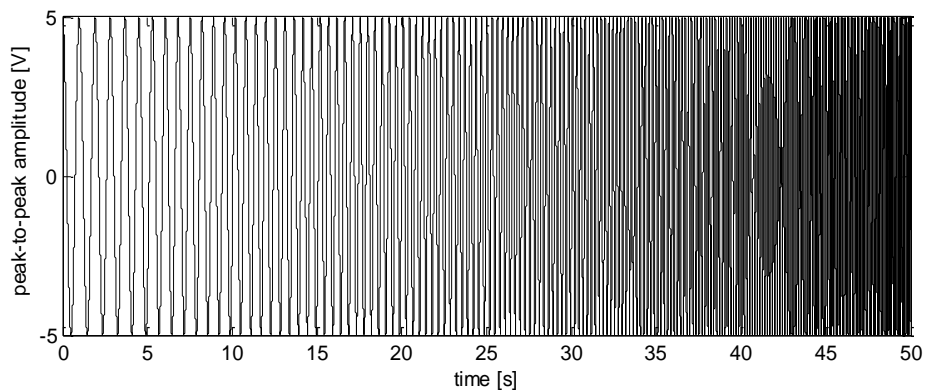


Figure 4.3 First 50 Seconds Time History of Input Signal

After the experiment is carried out and the output data is obtained, the Fast Fourier Transform (FFT) is applied using MATLAB's 'fft' command. FRF for each piezoelectric patch group is used in the system identification process to find the transfer function between piezoelectric patch group and the sensor and also the system matrices. So as to find the mathematical model of the system, 'fitsys' command of the MATLAB located in μ Analysis and Synthesis Toolbox [58] is used.

The resultant mathematical models are actually continuous time models. In order to design a controller which works in the SpeedGoat Real Time Target Machine, all of the blocks in the simulation must have discrete time values. Additionally, the controller should also be designed with discrete time controller design techniques. Therefore, for the controller design, the system matrices found in continuous time domain are converted into discrete time domain with the sampling frequency of 10000Hz. While converting the continuous system matrices to discrete system matrices, pole-zero matching method is used with MATLAB's 'c2d' command. This command maps the poles of the transfer function from s plane to z plane. The complex variables have relation as shown in Equation (4.1) [59].

$$z = e^{Ts} \quad (4.1)$$

Finally, the continuous [60] and discrete [59] systems are found as shown in Equations (4.2) and (4.3), respectively.

$$\begin{aligned} \dot{x}(t) &= Ax(t) + Bu(t) \\ y(t) &= C_c x(t) + D_c u(t) \end{aligned} \quad (4.2)$$

$$\begin{aligned} x(k+1) &= Gx(k) + Hu(k) \\ y(k) &= C_d x(k) + D_d u(k) \end{aligned} \quad (4.3)$$

Where;

x: State vector

u: Input Vector

y: Output Vector

A: Continuous Time State Matrix

B: Continuous Time Input Matrix

C: Output Matrix

D: Direct Transmission Matrix

G: Discrete Time State Matrix

H: Discrete Time Input Matrix

Subscripts 'c' and 'd' stand for continuous and discrete systems, respectively.

Equation (4.2) represents the whole system. However in this work, coupling effects are excluded and therefore the complete system is investigated for each actuator group separately. Following assumption is made for the continuous system matrices and applied in the discrete domain in the same manner. State vector is divided into three groups for each of the modes, input vector is also formed by three individual actuator groups as shown in Equation (4.4).

$$\begin{aligned}x &= \begin{bmatrix} x_1 \\ x_2 \\ x_3 \end{bmatrix} \\u &= \begin{bmatrix} u_1 \\ u_2 \\ u_3 \end{bmatrix} \\y &= y_1 + y_2 + y_3\end{aligned}\tag{4.4}$$

Although there is coupling between the actuator groups in the real system, they are treated as separate systems taking the off diagonal elements as zero as shown in Equation (4.5).

$$\begin{aligned}\dot{x}(t) &= \begin{bmatrix} A_1 & 0 & 0 \\ 0 & A_2 & 0 \\ 0 & 0 & A_3 \end{bmatrix} x(t) + \begin{bmatrix} B_1 & 0 & 0 \\ 0 & B_2 & 0 \\ 0 & 0 & B_3 \end{bmatrix} u(t) \\ y(t) &= [C_1 \quad C_2 \quad C_3]x(t) + [D_1 \quad D_2 \quad D_3]u(t)\end{aligned}\quad (4.5)$$

Subscripts 1, 2 and 3 in the equations (4.4) and (4.5) are for the subsystems. Combining equations (4.4) and (4.5), uncoupled system model is obtained and shown in Equation (4.6).

$$\begin{aligned}\begin{bmatrix} \dot{x}_1 \\ \dot{x}_2 \\ \dot{x}_3 \end{bmatrix} &= \begin{bmatrix} A_1 & 0 & 0 \\ 0 & A_2 & 0 \\ 0 & 0 & A_3 \end{bmatrix} \begin{bmatrix} x_1 \\ x_2 \\ x_3 \end{bmatrix} + \begin{bmatrix} B_1 & 0 & 0 \\ 0 & B_2 & 0 \\ 0 & 0 & B_3 \end{bmatrix} \begin{bmatrix} u_1 \\ u_2 \\ u_3 \end{bmatrix} \\ y(t) &= [C_1 \quad C_2 \quad C_3] \begin{bmatrix} x_1 \\ x_2 \\ x_3 \end{bmatrix} + [D_1 \quad D_2 \quad D_3] \begin{bmatrix} u_1 \\ u_2 \\ u_3 \end{bmatrix}\end{aligned}\quad (4.6)$$

Having uncoupled the system, Equation (4.6) can be divided into three equations and systems are calculated separately.

$$\begin{aligned}\dot{x}_1 &= A_1 x_1 + B_1 u_1 \\ y_1 &= C_1 x_1 + D_1 u_1\end{aligned}\quad (4.7)$$

$$\begin{aligned}\dot{x}_2 &= A_2 x_2 + B_2 u_2 \\ y_2 &= C_2 x_2 + D_2 u_2\end{aligned}\quad (4.8)$$

$$\begin{aligned}\dot{x}_3 &= A_3 x_3 + B_3 u_3 \\ y_3 &= C_3 x_3 + D_3 u_3\end{aligned}\quad (4.9)$$

State space matrices are found by the method described above, separately for each actuator group.

4.3.1 Transfer Function between the 1st Piezoelectric Actuator Patch Group and the Sensor

To find the response of the sensor to 1st Piezoelectric Actuator Patch Group (i.e. PZT patches of 1 to 4 in Figure 3.8) sine chirp is applied. Time domain history of the sensor due to sine chirp is shown in Figure 4.4. FFT analysis is then applied to this time data to find the FRF which is also shown in Figure 4.5.

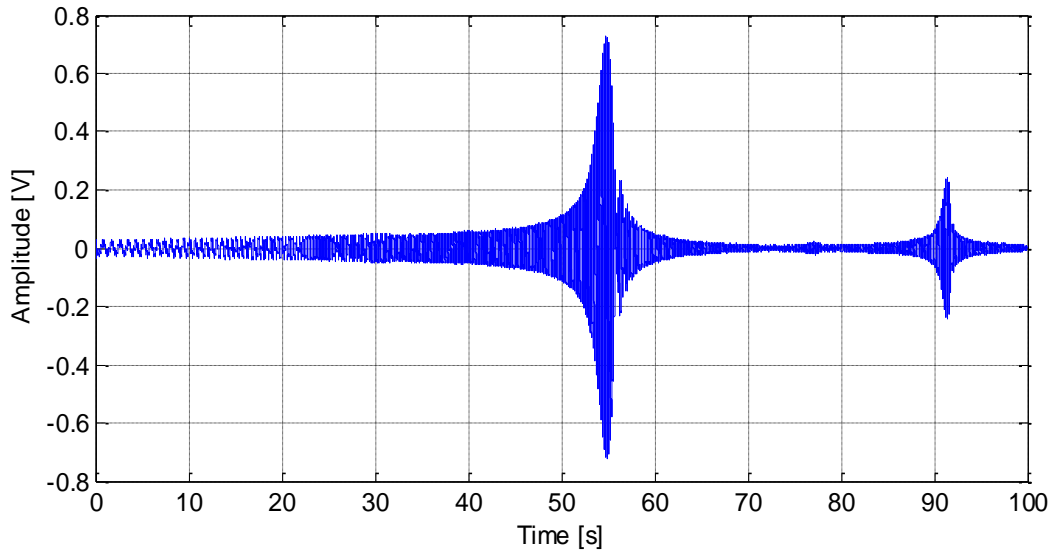


Figure 4.4 Response of the sensor to the 1st Piezoelectric Actuator Patch Group in Time Domain

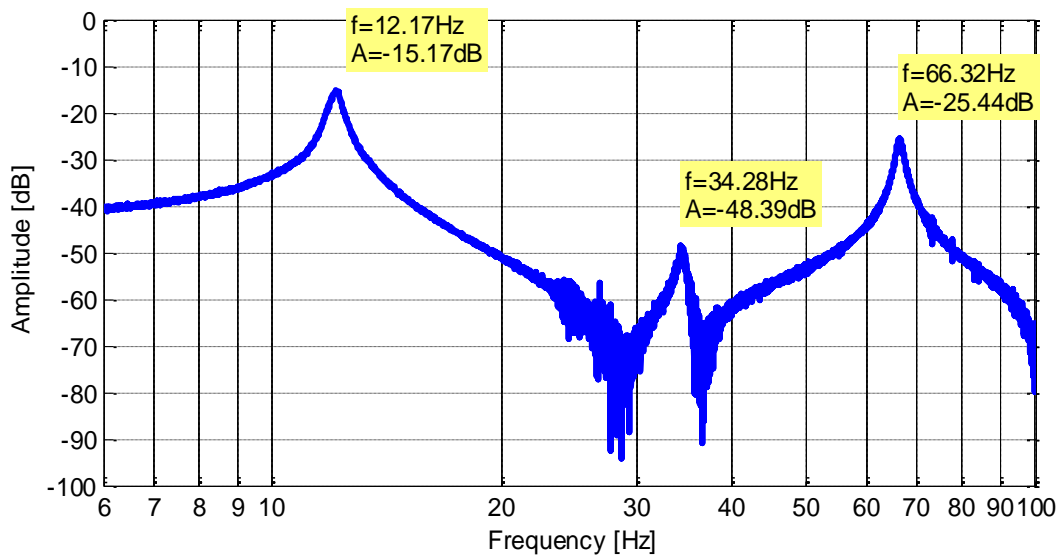


Figure 4.5 Frequency Response Function between the 1st Piezoelectric Actuator Patch Group and the Sensor

As it can clearly be seen that the maximum peak is in the 1st resonant frequency. The mathematical model system matrices corresponding to this FRF in continuous time domain is given in Equation (4.10). A system model covering only the first mode is enough to have for this case. Also note that, the 1st Piezoelectric Actuator Patch Group is located mainly for the first resonant frequency suppression. Thus, the system model

order of 2 is selected for this transfer function. The corresponding frequency response of this system model with the experimental data is shown in Figure 4.6.

$$\dot{x}_1(t) = \begin{bmatrix} -1.5310 & -76.1197 \\ 76.1197 & -1.3187 \end{bmatrix} x_1(t) + \begin{bmatrix} 0.5188 \\ -0.4726 \end{bmatrix} u_1(t) \quad (4.10)$$

$$y_1(t) = [0.5188 \quad 0.4726] x_1(t) + [4.1051 \times 10^{-4}] u_1(t)$$

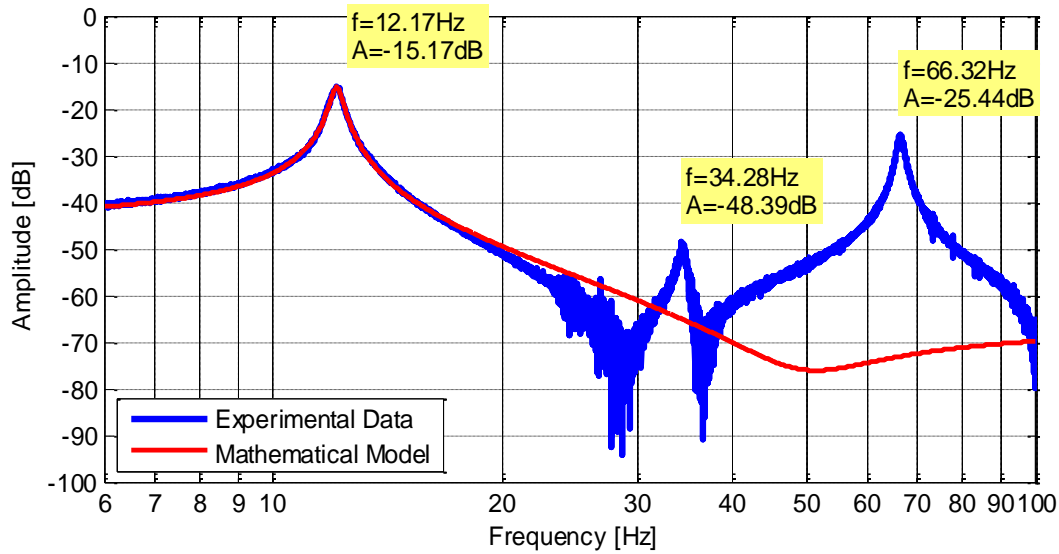


Figure 4.6 FRF for the 1st Piezoelectric Patch Group obtained by Mathematical Model and Experimental Data

After the system matrices for continuous time are found, they are converted into the discrete time using Equation (4.1) with sampling rate, T, of 1/10000 seconds (Equation (4.11)).

$$x_1(k+1) = \begin{bmatrix} 0.9998 & 1 \\ -5.7924 \times 10^{-5} & 0.9998 \end{bmatrix} x_1(k) + \begin{bmatrix} 0 \\ 1.7139 \times 10^{-3} \end{bmatrix} u_1(k) \quad (4.11)$$

$$y_1(k) = [2.1723 \times 10^{-4} \quad 2.8899 \times 10^{-3}] x_1(k) + [4.1284 \times 10^{-4}] u_1(k)$$

4.3.2 Transfer Function between the 2nd Piezoelectric Actuator Patch Group and the Sensor

For the second controller group (i.e. PZT patches of 5 to 8 in Figure 3.8), to obtain the response of the sensor to the 2nd Piezoelectric Actuator Patch Group, a sine chirp is applied again. The time domain history of the sensor due to applied sine chirp is shown in Figure 4.7. As expected, different than the first group response, the response of the second actuator group for second mode is relatively high since these piezoelectric patches are located mainly to control the second mode of the Smart Sandwich Plate. FFT analysis is then applied to this time data in order to find the FRF which is shown in Figure 4.8. The 2nd order system is fitted to the frequency domain data and the system matrices for this particular case are given in Equation (4.12). The frequency response of this system model with the experimental data is shown in Figure 4.9. The sampling rate of 1/10000 seconds are used again to convert the continuous system matrices into discrete ones (Equation (4.13)).

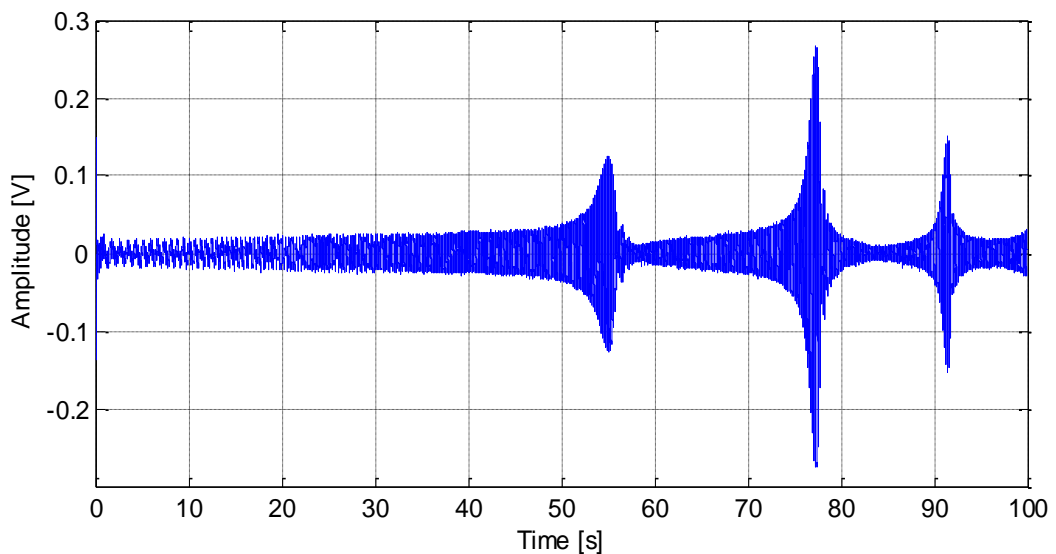


Figure 4.7 Response of the sensor to 2nd Piezoelectric Actuator Patch Group in Time Domain

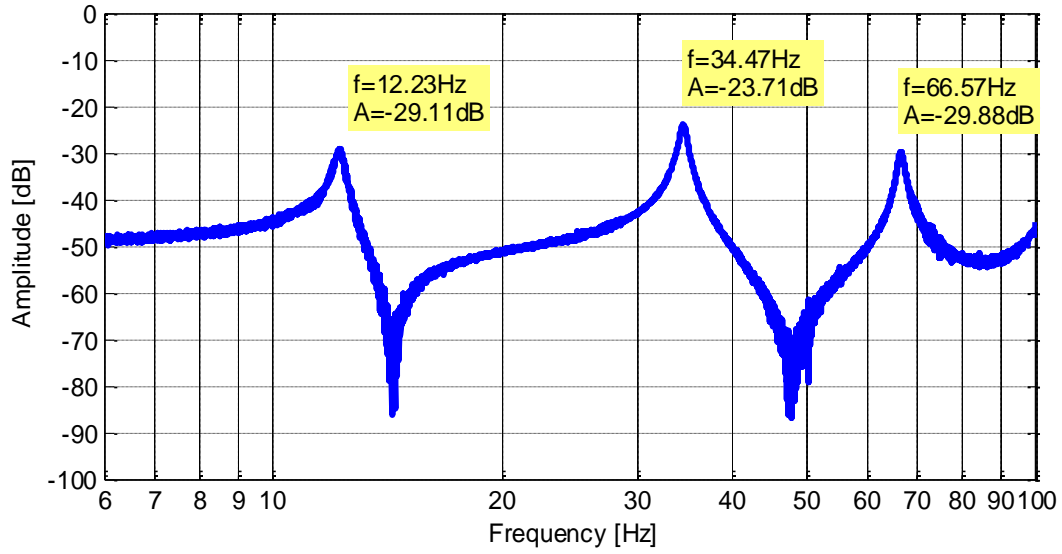


Figure 4.8 FRF between the 2nd Piezoelectric Actuator Patch Group and the Sensor

$$\dot{x}_2(t) = \begin{bmatrix} -2.5883 & -216.6807 \\ 216.6807 & -2.5951 \end{bmatrix} x_2(t) + \begin{bmatrix} 0.4068 \\ -0.4025 \end{bmatrix} u_2(t) \quad (4.12)$$

$$y_2(t) = [0.4068 \quad 0.4025] x_2(t) + [1.1894 \times 10^{-4}] u_2(t)$$

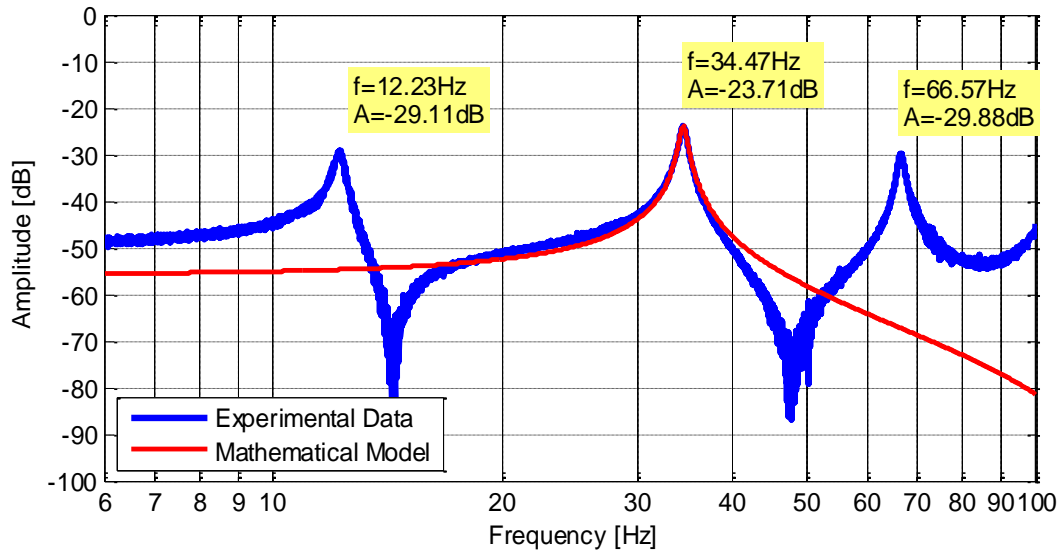


Figure 4.9 FRF for the 2nd Piezoelectric Patch Group obtained by Mathematical Model and Experimental Data

$$x_2(k+1) = \begin{bmatrix} 0.9995 & 1 \\ -4.6919 \times 10^{-4} & 0.9995 \end{bmatrix} x_2(k) + \begin{bmatrix} 0 \\ 1.6154 \times 10^{-3} \end{bmatrix} u_2(k) \quad (4.13)$$

$$y_2(k) = [4.3885 \times 10^{-4} \quad 6.5518 \times 10^{-4}] x_2(k) + [1.1918 \times 10^{-4}] u_2(k)$$

4.3.3 Transfer Function between the 3rd Piezoelectric Actuator Patch Group and the Sensor

For the third controller group (i.e. PZT patches of 9 to 12 in Figure 3.8), to obtain the response of the sensor to the 3rd Piezoelectric Actuator Patch Group, the same procedure is followed via applied sine chirp and the time domain history of the sensor is shown in Figure 4.10.

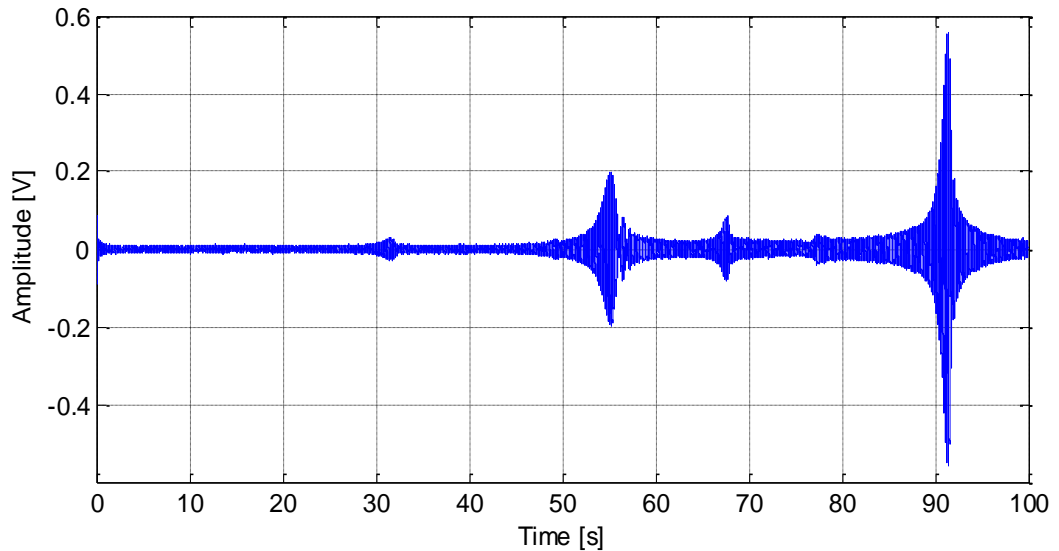


Figure 4.10 Response of the sensor to 3rd Piezoelectric Actuator Patch Group in Time Domain

Similar to the second controller group, response of the third actuator group for the third mode is relatively high since these piezoelectric patches are located mainly to control the third mode of the Smart Sandwich Plate. FFT analysis is then applied to this time data in order to find the FRF shown in Figure 4.11.

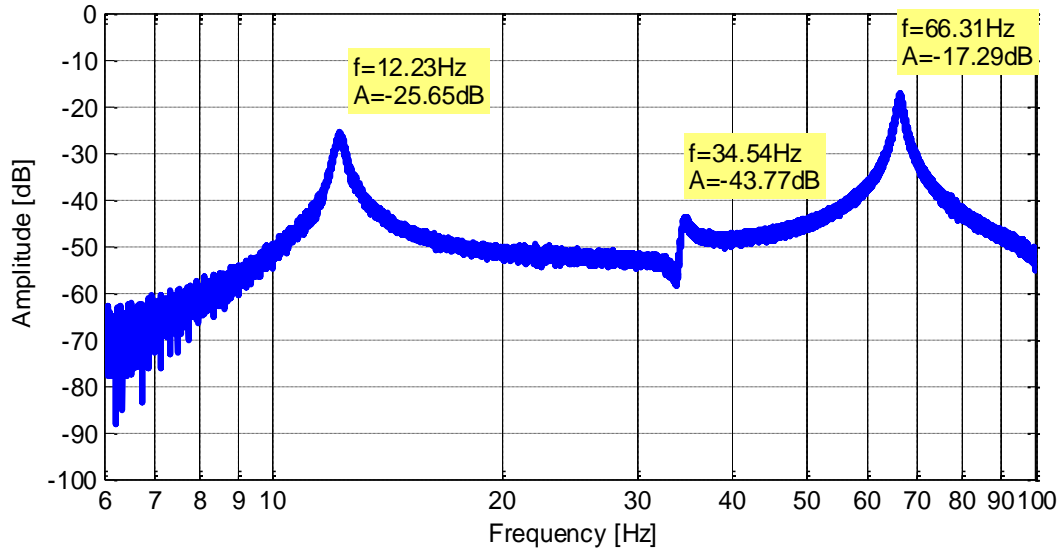


Figure 4.11 FRF between the 3rd Piezoelectric Actuator Patch Group and the Sensor

Again a system model with 2nd order is selected covering only 3rd mode. System model is given in Equation (4.14). The frequency response of this system model with the experimental data is shown in Figure 4.12. After the system matrices for continuous time are found, they are converted into the discrete time with sampling rate of 1/10000 seconds Equation (4.15).

$$\dot{x}_3(t) = \begin{bmatrix} -8.8465 & -416.5238 \\ 416.5238 & -0.1734 \end{bmatrix} x_3(t) + \begin{bmatrix} -1.0388 \\ 0.1450 \end{bmatrix} u_3(t) \quad (4.14)$$

$$y_3(t) = [-1.0388 \quad -0.1450] x_3(t) + [9.6843 \times 10^{-4}] u_3(t)$$

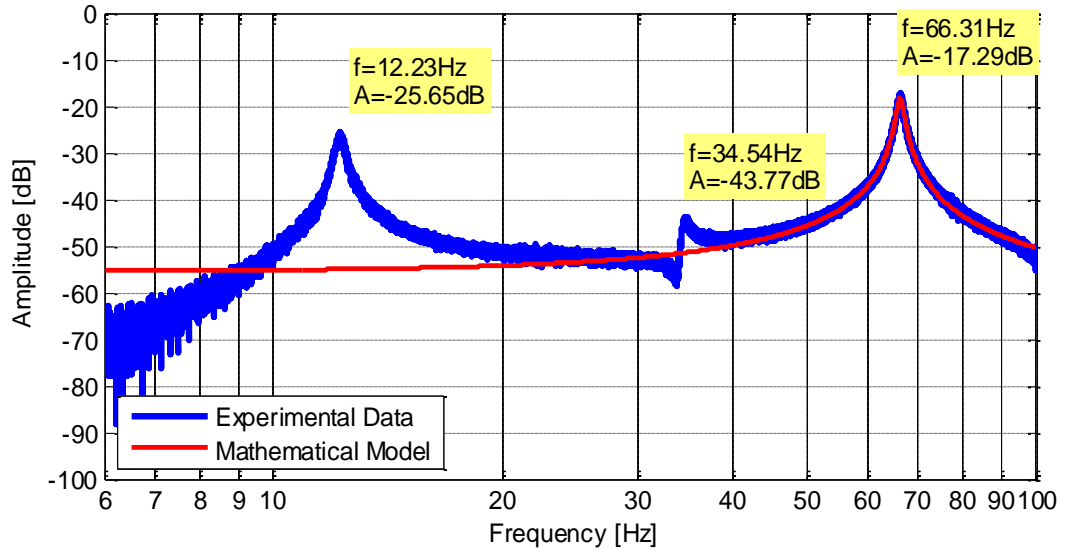


Figure 4.12 FRF for the 3rd Piezoelectric Patch Group obtained by Mathematical Model and Experimental Data

$$x_3(k+1) = \begin{bmatrix} 0.9987 & 1 \\ -1.7321 \times 10^{-3} & 0.9987 \end{bmatrix} x_3(k) + \begin{bmatrix} 0 \\ 0.0101 \end{bmatrix} u_3(k) \quad (4.15)$$

$$y_3(k) = [1.0092 \times 10^{-4} \quad 0.0106] x_3(k) + [1.0224 \times 10^{-3}] u_3(k)$$

4.4 Conclusion

Finally, in this section, the system matrices for each of the piezoelectric actuator groups are found and the amplitude of the resonant peaks for each group are presented in Table 4.1.

Table 4.1 Comparison of the Amplitude of the Resonant Peaks due to Excitation of Each Piezoelectric Actuator Group

	Amplitude at ω_1	Amplitude at ω_2	Amplitude at ω_3
	[dB]	[dB]	[dB]
Actuator Group 1	-15.17	-48.39	-25.44
Actuator Group 2	-29.11	-23.71	-29.88
Actuator Group 3	-25.65	-43.77	-17.29

Looking at Table 4.1, it is clear that, maximum amplitude of each modes occurs due to the excitation of their own actuator groups. Having found the system matrices of the system for all actuators, the design of the controllers will be the next action to be taken.

Additionally, a comparison between the experiments which are performed before and after the piezoelectric actuators and sensors are attached to investigate how the patches are affecting the resonance frequencies. In below table, the results are provided.

Table 4.2 Comparison of the Resonance Frequencies before and after PZT Attachment

	ω_1	ω_2	ω_3
	[Hz]	[Hz]	[Hz]
EMA	11.53	33.94	71.11
Piezoelectric Group 1	12.17	34.28	66.32
Piezoelectric Group 2	12.23	34.47	66.57
Piezoelectric Group 3	12.23	34.54	66.31

CHAPTER 5

ACTIVE VIBRATION CONTROL OF THE SMART SANDWICH PLATE

5.1 Introduction

In this chapter, a controller is designed for an active vibration control and its experimental application on the smart sandwich plate is performed. First a pole placement type controller is designed for each of the piezoelectric actuator groups. In order to complete the pole placement type controller design, state observers are also designed. After the design procedure is completed, experimental cases of forced and free vibration are applied. For free vibration case, time to finish all vibrations is tried to be shortened with controller. On the other hand, in forced vibration cases, amplitude due to the disturbance signal is tried to be lowered.

5.2 Design of the Active Vibration Controller

In order to control this vibratory system, pole placement is chosen to be the controller. In this type controller, closed loop poles can be chosen to determine the damping ratio and undamped natural frequency [60]. State equation of the system to be controlled is given in Equation (5.1) [59].

$$x(k + 1) = Gx(k) + Hu(k) \quad (5.1)$$

where

$x(k)$: State vector (n-vector) at k^{th} sampling instant

$u(k)$: Control Signal (scalar) at k^{th} sampling instant

G : $n \times n$ Matrix

H : $n \times 1$ Matrix

Having chosen the controller signal $u(k)$ as $-Kx(k)$, where K is the state feedback gain matrix, the closed loop system can be illustrated with block diagram shown in Figure 5.1.

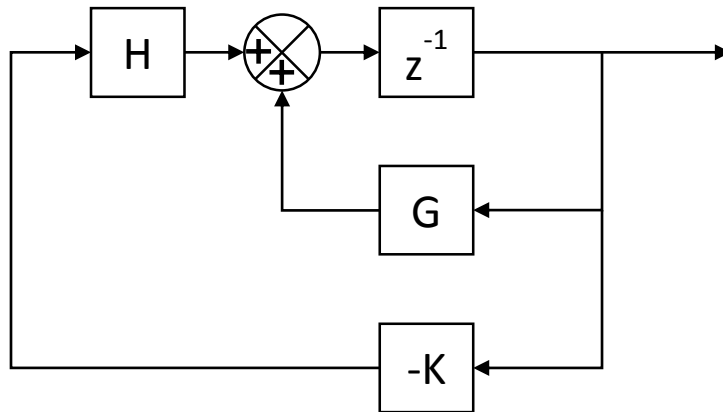


Figure 5.1 Block Diagram of State Feedback Control System

Coefficients of the gain matrix, K , are found by MATLAB's 'place' command. The inputs of this command are G , H matrices and the desired poles of the system. After the desired pole locations are decided, K is found to have poles of the system at the determined locations. In the controller design problem, pole locations are determined not to change the natural frequency locations but the damping ratios. Poles of the system are related to natural frequencies and damping ratios with equation (5.2).

$$p = -\omega_n \zeta \pm \omega_n \sqrt{1 - \zeta^2} \quad (5.2)$$

where

p : Pole of the system

ω_n : Natural frequency of the system

ζ : Damping Ratio

While designing the pole location, first the current natural frequencies and damping ratios are found. After that, the damping ratio is increased until the physical limits of the experimental system permit. Using this procedure, all controller groups are designed.

Notice that the real system is like a black box that gives only the response of the output to input signal. Therefore, the states of the system cannot be measured. Although the states are not available directly, an observer can estimate them. Block diagram of both Plant and Controller-Observer is given in Figure 5.2. L matrix is the observer gain matrix and found similar to K using transpose of G and C_d matrices. Poles of the observer gain matrix is found by multiplying the poles of the controller gain matrix by 5 to have the observer 5 times faster than the system.

The experimental system is noisy unlike to the simulation environment. Therefore some high frequency noise affects the system negatively. Controller may diverge while trying to control the high frequency modes other than the modes of interest. In order to prevent this phenomenon, a band pass filter is designed to filter the frequencies different than the control interval. Filter is placed between the plant output and the controller input. Filters are different for each of the controller groups.

Design of the controller is based mainly on the damping ratio to be increased. The damping ratio is found by Equation (5.2) and it is multiplied by a number found iteratively. Design restriction is selected compulsorily to have the controller response signal less than the capacity of SpeedGoat Real Time Target Machine with a safety margin.

Table 5.2 Gain Matrices of the Controllers and the Observers

	Controller Gain Matrix	Observer Gain Matrix
Controller Group 1	$[-8.3260 \times 10^{-5} \quad 0.4154]$	$\begin{bmatrix} -56.3450 \\ 6.3381 \end{bmatrix}$
Controller Group 2	$[-3.7368 \times 10^{-4} \quad 0.5128]$	$\begin{bmatrix} 1.5481 \\ 25.5460 \end{bmatrix}$
Controller Group 3	$[-1.5535 \times 10^{-3} \quad 0.7103]$	$\begin{bmatrix} -2061.2789 \\ 27.1798 \end{bmatrix}$

Filters are designed to reject the experimental noise. However it is necessary to allow frequencies around the resonance peaks in order not to detract from the performance. Transfer functions of the filters are designed not only to have neither increase nor decrease in the response of the sensor at the resonant frequencies but also to lower the amplitudes at frequencies that give both low and high frequency noise content. Thus, filters for each groups allows data transition around resonant frequency.

The transfer function of the filter for the 1st controller group is given in equation (5.3). Moreover, bode diagram of the filter is given in Figure 5.3 to see the frequency interval which is influenced.

$$F(s) = \frac{1.301 \times 10^5 s + 6506}{s^3 + 720s^2 + 134000s + 2.4 \times 10^6} \quad (5.3)$$

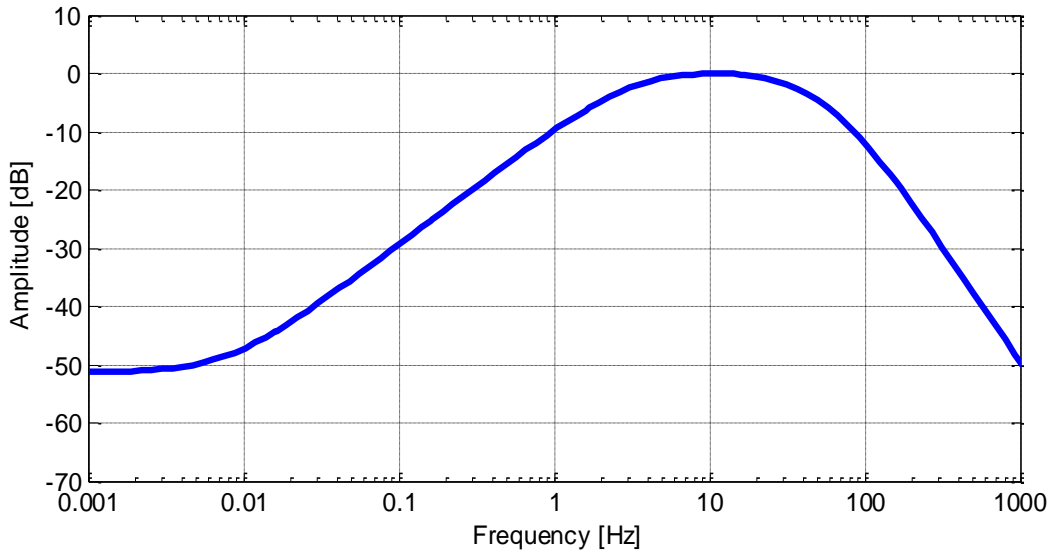


Figure 5.3 Bode Diagram of the Band Pass Filter for 1st Controller Group

The transfer functions of the filter for the 2nd and 3rd controller groups are given in equations (5.4) and (5.5). Furthermore, bode diagram of the filters are given in Figure 5.4 and Figure 5.5, respectively, so as to see the frequency that are passed.

$$F(s) = \frac{9.272 \times 10^5 s + 46361}{s^3 + 1920s^2 + 938000s + 1.8 \times 10^7} \quad (5.4)$$

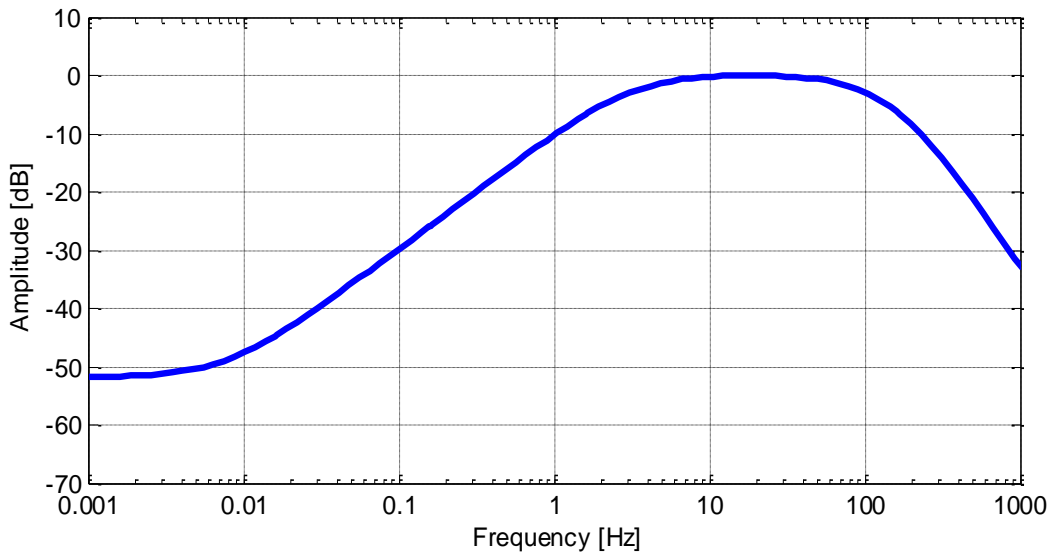


Figure 5.4 Bode Diagram of the Band Pass Filter for 2nd Controller Group

$$F(s) = \frac{1.028 \times 10^6 s + 51423}{s^3 + 2020s^2 + 1040000s + 2 \times 10^7} \quad (5.5)$$

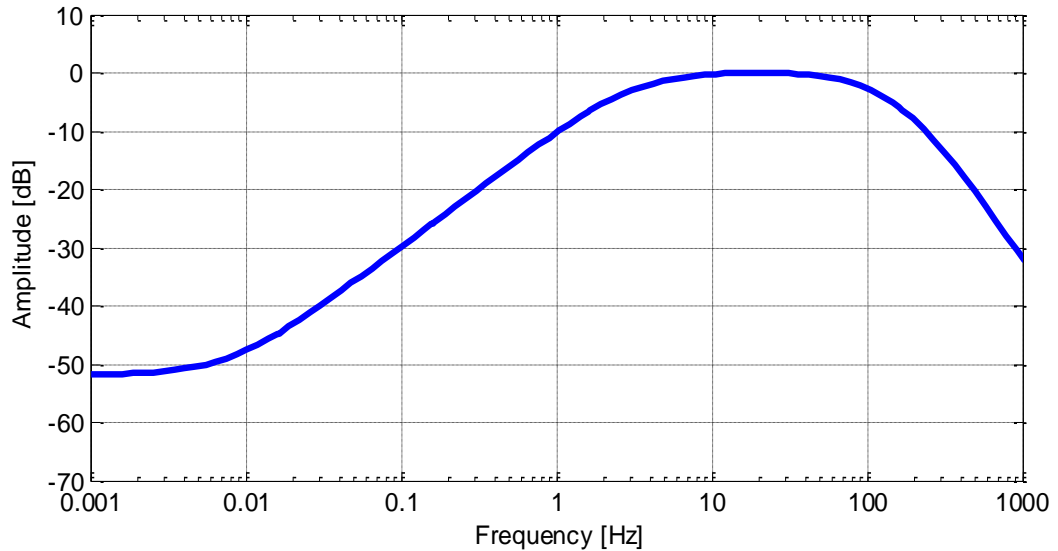


Figure 5.5 Bode Diagram of the Band Pass Filter for 3rd Controller Group

Although bode diagrams of the filters look almost the same, they have different passing frequency values. Filters reject the corresponding off-resonance frequencies.

In order to show that the designed controllers are working, first, the system is simulated and the following experimental case studies are performed. In the simulations, it is shown that the controllers are performing well inside the physical limits of the experimental setup and it is ensured that the vibration suppression is provided. In the experimental case studies, free and forced vibrations are aimed to be suppressed.

5.3 Simulations for Active Vibration Control

5.3.1 System Modelling of the Plant

In Chapter 4, system identification of the controller groups is completed. Nevertheless, in order to simulate the system completely, it is necessary to determine

the transfer functions for the whole system. Since all of the transfer functions for controllers are known, it is only needed to find a transfer function between disturbance actuator (represented with 'D' in Figure 3.9) and the sensor. Same procedure used in Chapter 4 is operated to come up with the frequency domain data of the sensor output owing to the disturbance input. First, a sine chirp is applied through the disturbance actuator. FFT analysis is then performed on the recorded time domain history of the sensor. By taking this frequency domain data, a system model of order six is composed to cover the first three modes of the Smart Sandwich Plate. Discrete system matrices with 10 kHz sampling time is given in equation (4.11). Figure 5.6 demonstrates the FRF for the disturbance patch obtained by mathematical model and experimental data. Having found the plant model shown in Figure 5.7, simulation model is also constructed (Figure 5.8).

$$\begin{aligned}
 G &= \begin{bmatrix} 0.9987 & 1 & 0 & 0 & 0 & 0 \\ -0.0017 & 0.9987 & 5.0627 \times 10^{-4} & 0.0129 & -3.6200 \times 10^{-5} & 0.0114 \\ 0 & 0 & 0.9995 & 1 & 0 & 0 \\ 0 & 0 & -4.6918 \times 10^{-4} & 0.9995 & -3.6790 \times 10^{-5} & 0.0116 \\ 0 & 0 & 0 & 0 & 0.9999 & 1 \\ 0 & 0 & 0 & 0 & -5.8382 \times 10^{-5} & 0.9999 \end{bmatrix} \\
 H &= \begin{bmatrix} 0 \\ 0.0035 \\ 0 \\ 0.0036 \\ 0 \\ 0.0032 \end{bmatrix} \\
 C_d &= [-1.7584 \times 10^{-4} \quad 0.0036 \quad 1.4399 \times 10^{-4} \quad 0.0037 \quad -1.0296 \times 10^{-5} \quad 0.0032] \\
 D_d &= 0.0010
 \end{aligned} \tag{5.6}$$

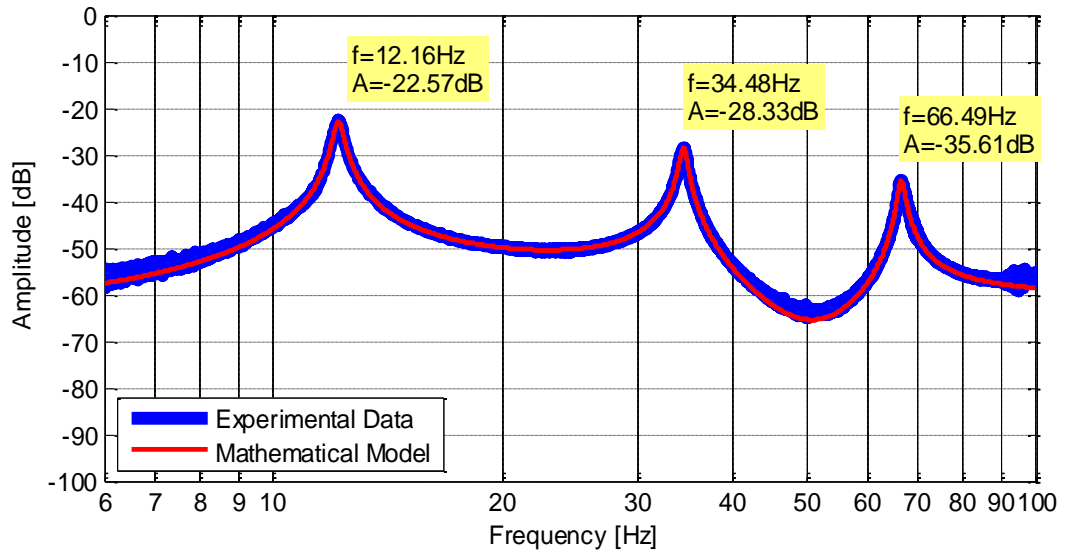


Figure 5.6 FRF for the Disturbance Patch obtained by Mathematical Model and Experimental Data

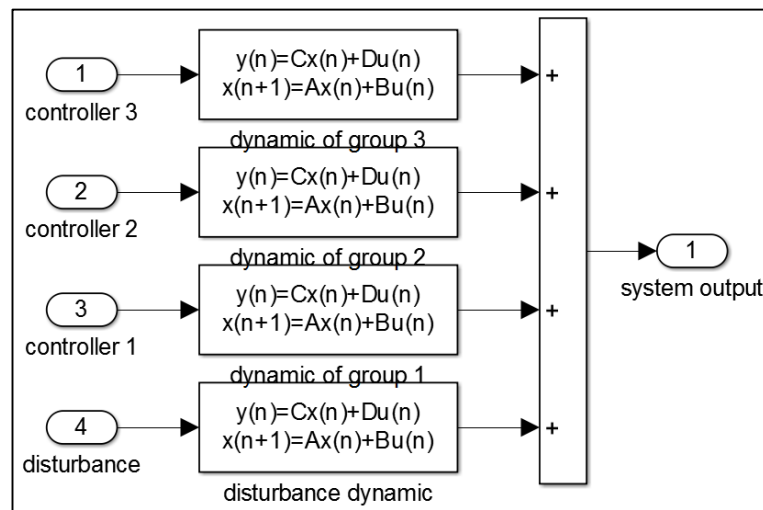


Figure 5.7 Plant Model

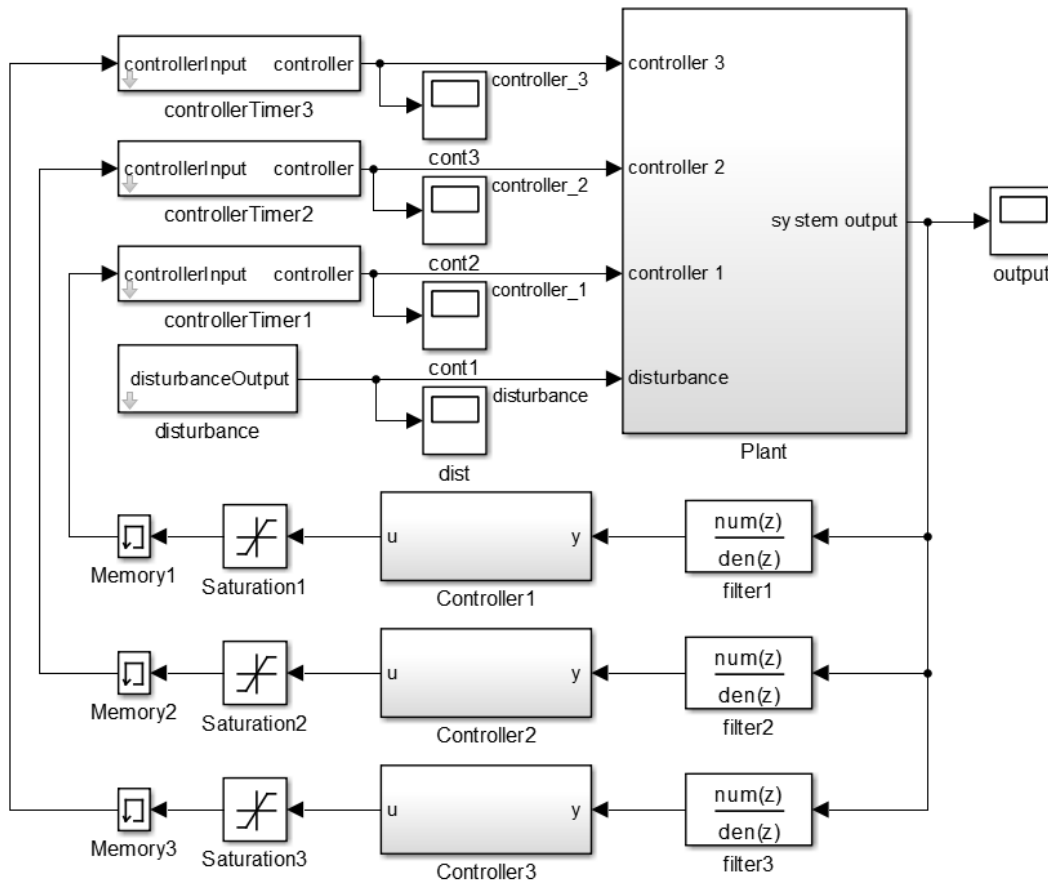


Figure 5.8 System Simulation

5.3.2 Simulation Results of Active Vibration Control of the Smart Sandwich Plate

Before performing an experiment, a system simulation is needed to indicate that the arranged controllers are working properly. In simulations, free and forced vibration cases are observed. In order to verify controller Group 1, free vibration condition is tested first. To have a free vibration in simulation, plate is release to create approximately 0.6 V and it takes 5.3 seconds to come to rest completely without controllers. Same case is repeated with controller Group 1 is on and it takes 1.8 seconds to stop completely. As a result, controller Group 1 provides a 74% acquisition in free vibration case as shown in Figure 5.9. In the simulation, as well as in the experiment, it is practically not feasible to observe the system having a zero amplitude

continuously; therefore, the stopping criteria for the free vibration case is chosen as to have an oscillation less than the sensor noise level.

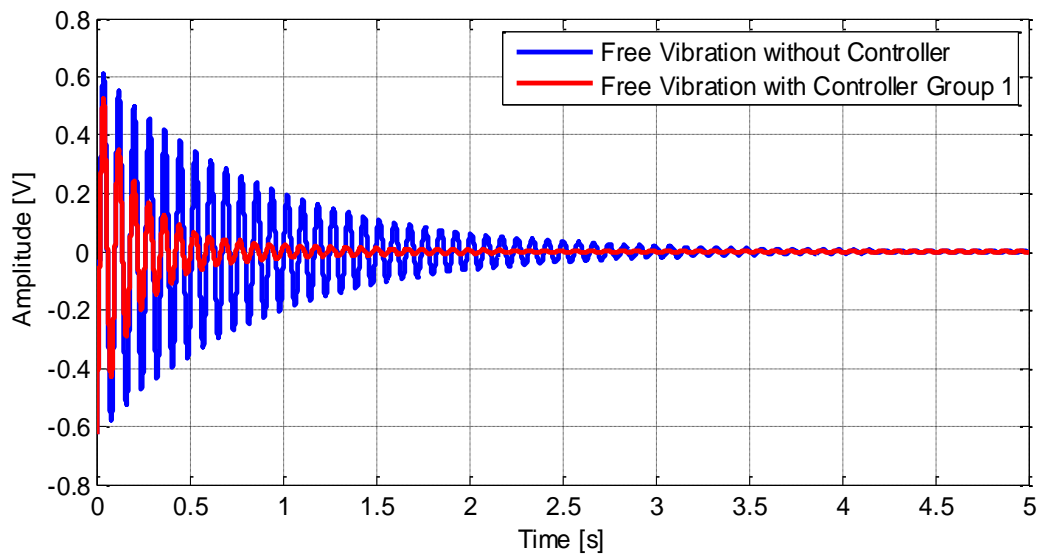


Figure 5.9 Active Vibration Control of the Plate due to an Initial Condition

The first mode suppression is demonstrated by constructing a disturbance signal at the first natural frequency of the Smart Sandwich Plate and operating the controller Group 1. For visualization of the situation, disturbance signal is given for a period of 20 s and the controller is activated at the 10th second. In Figure 5.10, controller performance for the 1st mode is represented. In addition, the controller output is also given in Figure 5.11 to show that it behaves inside its physical limits.

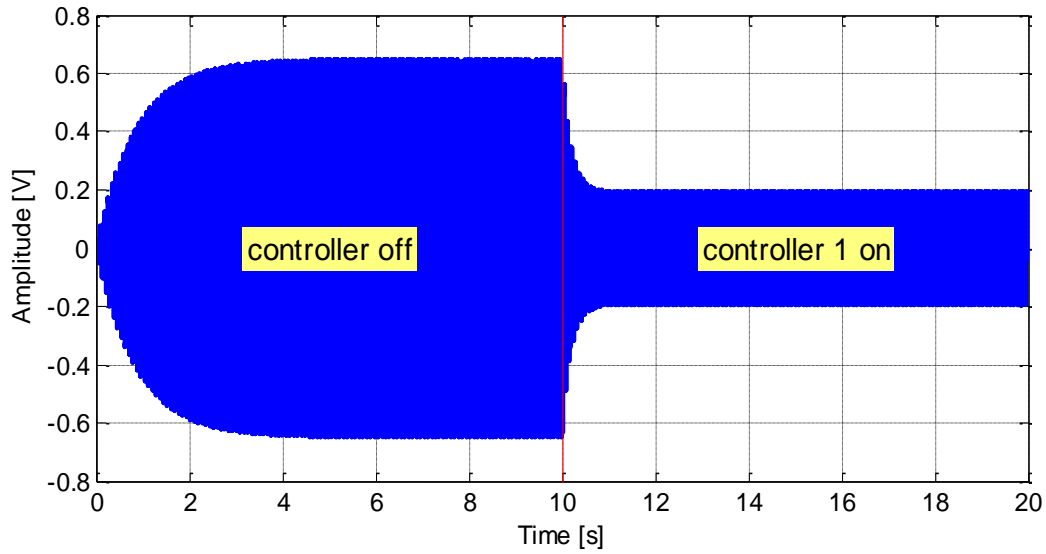


Figure 5.10 Active Vibration Control of the Plate due to an External Force at the 1st Natural Frequency

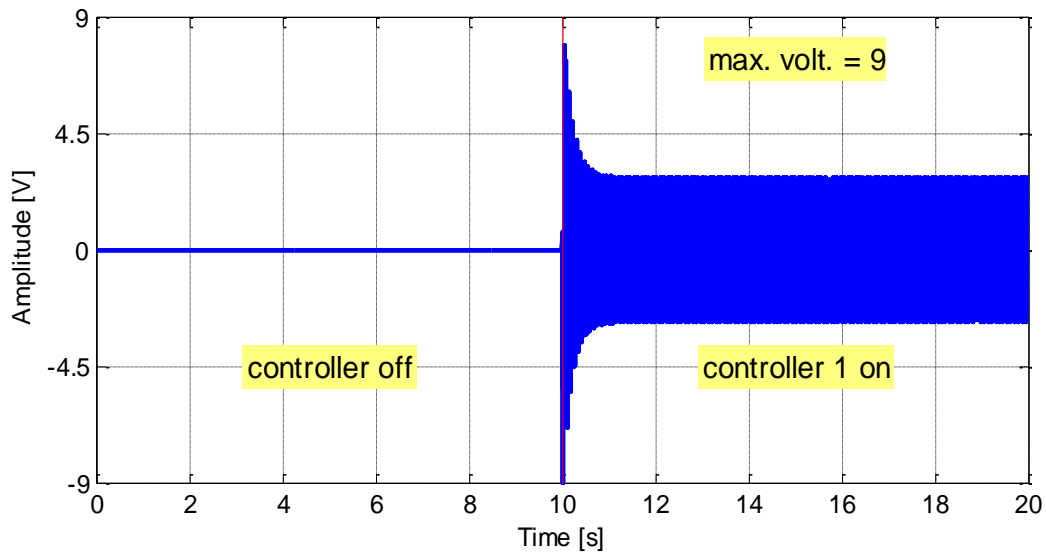


Figure 5.11 Controller Output to Suppress Vibration at the 1st Mode

For the second mode control, same system is simulated at the 2nd natural frequency of the plate. Disturbance signal is given to excite the second mode of the plate for 20 s and controller Group 2 is switched on at the 10th second. In Figure 5.12, performance of the controller for the 2nd mode is indicated. In addition, the controller output is also given in Figure 5.13 to show that it is also performing within the physical restrictions. Similar procedure is also practiced for the 3rd mode. Controller

performance and the controller output are shown in Figure 5.14 and Figure 5.15, respectively.

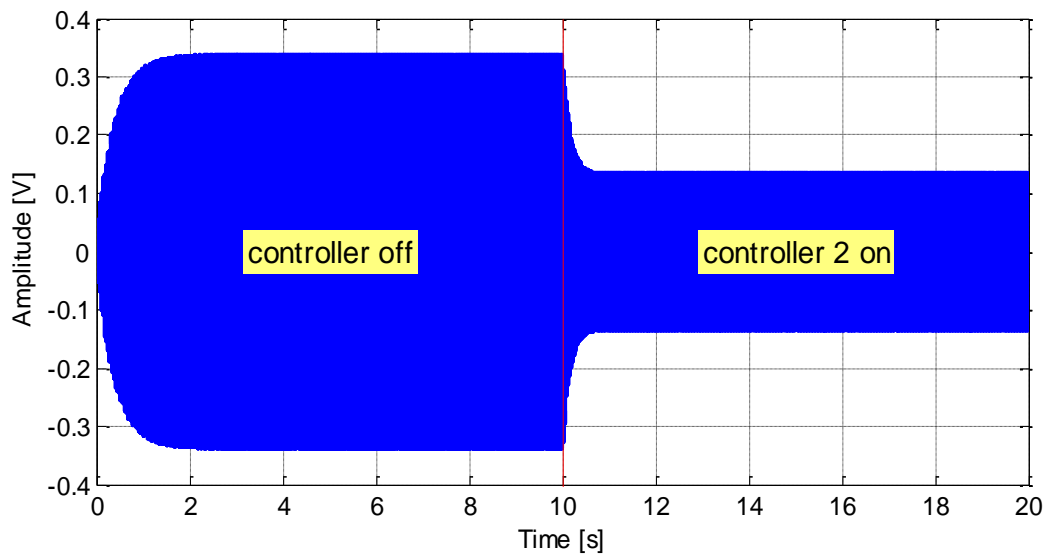


Figure 5.12 Active Vibration Control of the Plate due to an External Force at the 2nd Natural Frequency

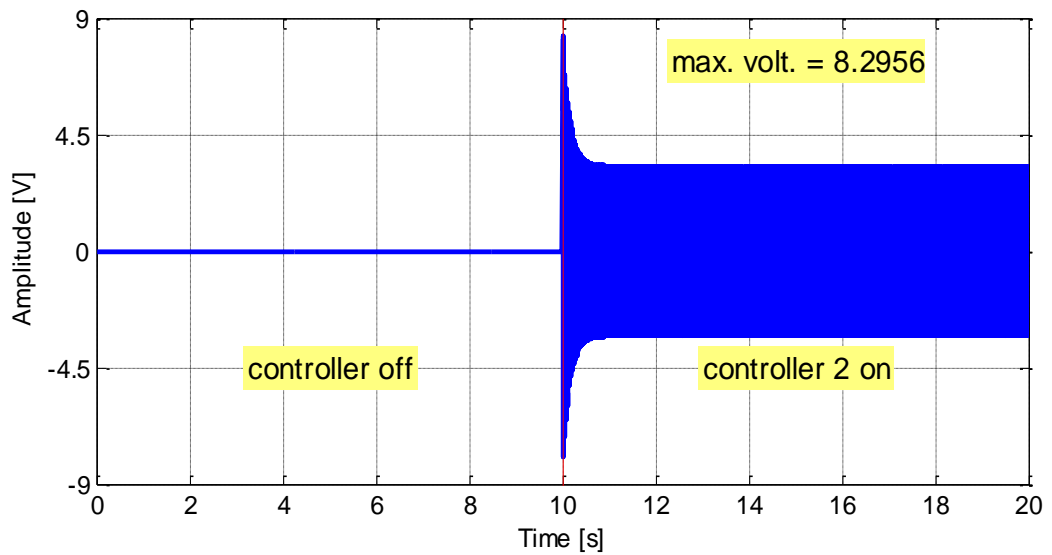


Figure 5.13 Controller Output to Suppress Vibration at the 2nd Mode

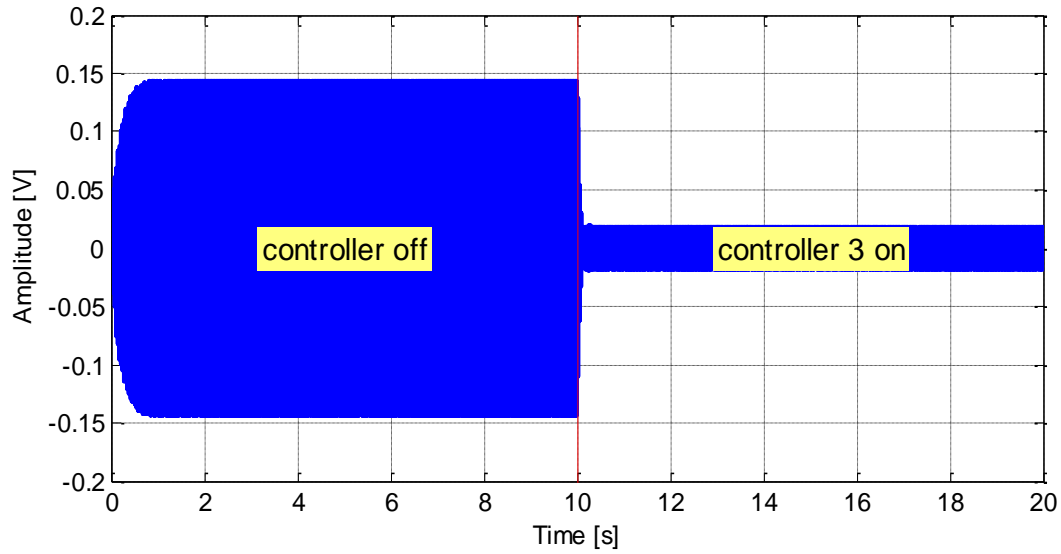


Figure 5.14 Active Vibration Control of the Plate due to an External Force at the 3rd Natural Frequency

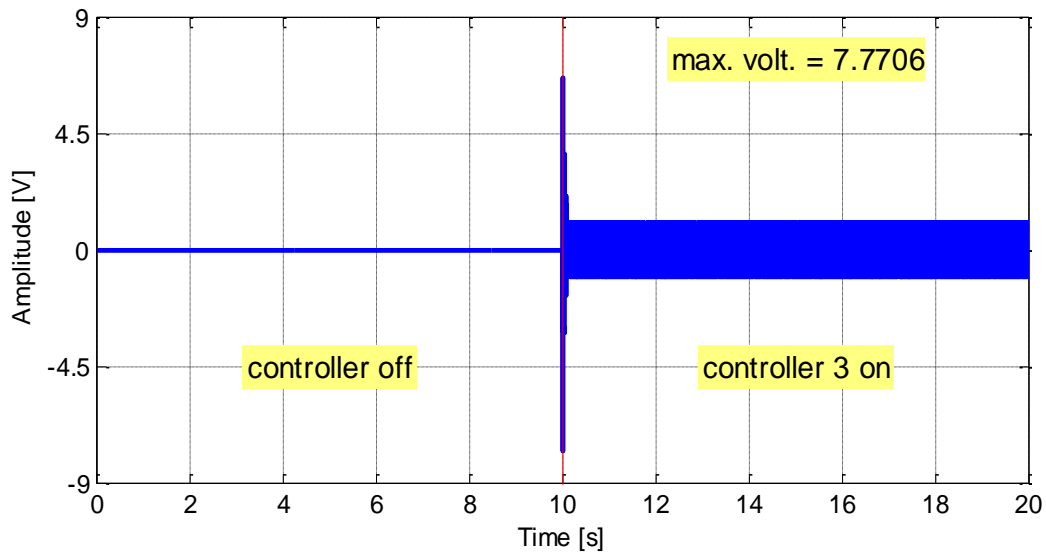


Figure 5.15 Controller Output to Suppress Vibration at the 3rd Mode

After validating the controllers which are working for their corresponding modes effectively, a sine chirp is given and the system is simulated to display the attenuation levels in the frequency domain as well. Standing inside the physical limits of the experimental setup, controllers are worked together and for all of the individual modes, suppression of the vibration is achieved (Figure 5.16). From the obtained simulation results, attenuation levels are also found and represented in Table 5.3.

When the third peak is considered, it can easily be shown that the resonance frequency changed up to 5 Hz. In the simulation, if the third filter is removed from the system the third frequency decreases to 67.64 Hz which is close to the third resonance frequency of the uncontrolled system.

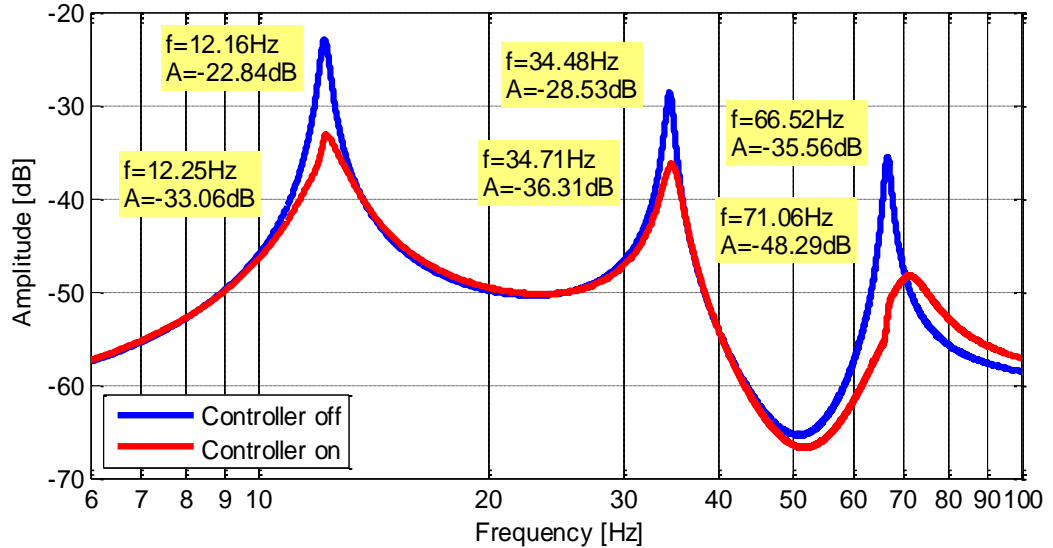


Figure 5.16 Simulated Controller Performances in Frequency Domain

Table 5.3 Simulated Attenuation Levels of Each Mode

Attenuation levels [dB]	
Mode 1	10.22
Mode 2	7.78
Mode 3	12.73

However, one should take into account that coupling effects (i.e. in the case when all the controllers are used together) may not be emulated splendidly in these simulations especially for the controllers with low order system models. In fact, the off-diagonal elements in Equation (4.6) are not zero in actual case. Therefore, the actual coupling of the controllers should be identified via experimental techniques and presented various real life case studies.

5.4 Case Study 1: Active Vibration Control of the Plate due to an Initial Condition: Free Vibration Suppression

Having satisfactorily and successfully obtained the results from simulations, similar cases are tested experimentally as well. In order to investigate the active vibration control performance of the Smart Sandwich Plate without any force acting on, i.e. free vibration case, oscillations of the plate due to an initial displacement is observed with and without controller force is acting. In the first case, plate is released with approximately 2 mm tip deflection from the centre of the top edge and time to stop is measured as 5.4 s. In the second case, plate is released with the same amount and the controller Group 1 is activated. Consequently, time to stop is measured as 1.4 s which means that the controller decrease the stopping time with 75% efficiency. Finally, the plate is released when all of the controllers are on. Run-down time reduced slighter than (approximately 1.1 s that means 80% drop in time) the case where one controller is on. Amplitudes of the motion are measured in Voltage units and the response graph in time domain is shown in Figure 5.17.

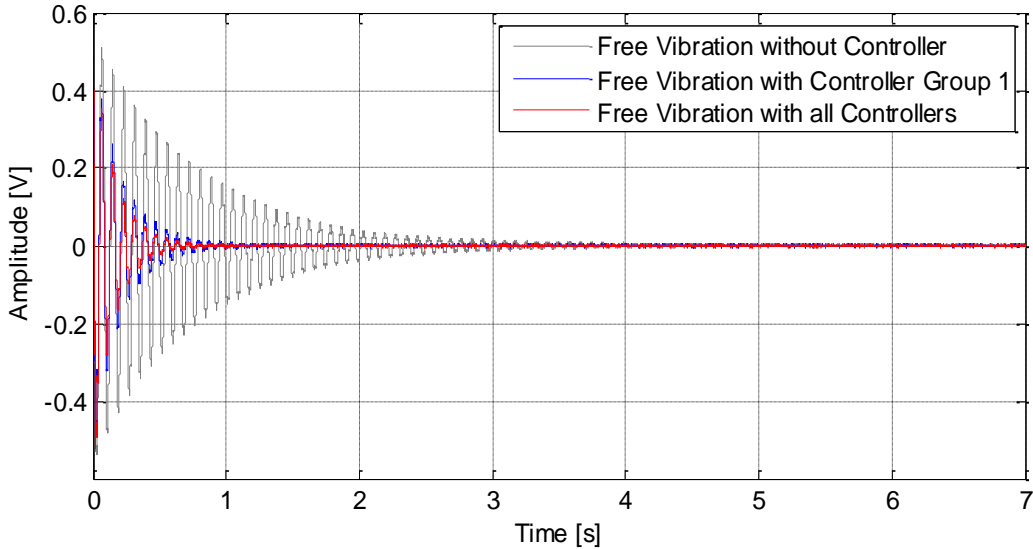


Figure 5.17 Active Vibration Control of the Plate due to an Initial Condition

In order to see the effects of the controllers 2 and 3, they are tested to suppress free vibration with controller 1. In Table 5.4, the summary of the results are shown.

Table 5.4 Free Vibration Suppression Durations

	Attenuation Time	Decrease Percentage
	[s]	[%]
No Controller	6.20	-
Group 1	1.60	74
Groups 1 + 2	1.55	75
Groups 1 + 3	1.25	80
Groups 1 + 2 + 3	1.20	81

5.5 Case Study 2: Active Vibration Control of the Plate due to an External Force: Force Vibration Suppression

5.5.1 Sinusoidal Signals at Resonant Frequencies

Unlike to the free vibration case, forced vibration suppression is performed against another vibratory signal which is a sine signal at the corresponding resonance frequency given by the disturbance piezoelectric patch (labelled as ‘D’ in Figure 3.9).. In the experiments, time required to reach the steady state value of the sensor response is decided as 10 seconds. In the resultant graphs, forced vibration with 9 V is applied to the plate and at 10th second, the controller begins operating. In Figure 5.18, controller performance for the 1st mode is represented. Additionally, the controller output is also given in Figure 5.19 to show that it performs near its physical boundaries.

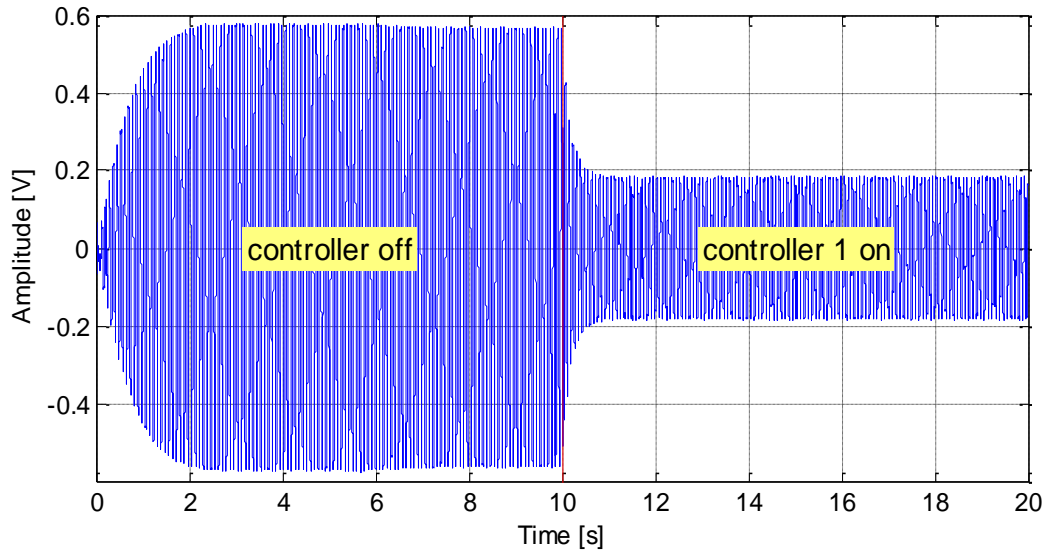


Figure 5.18 Active Vibration Control of the Plate due to an External Force at the 1st Resonance Frequency

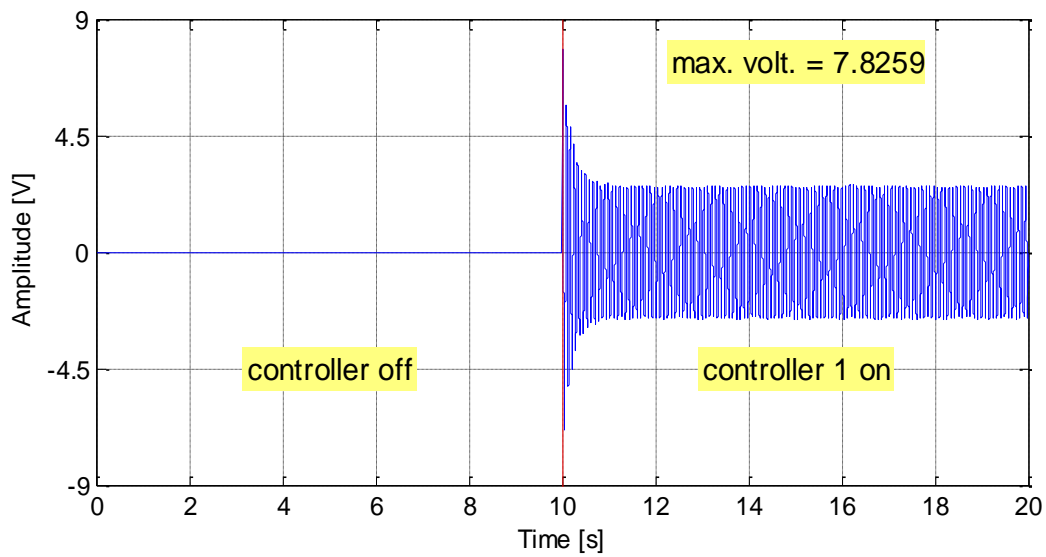


Figure 5.19 Controller Output to Suppress the 1st Mode Vibration

For the second mode control, same experiment is performed. This time the controller Group 2 is activated and the disturbance signal is given to trigger the second mode of the plate. In Figure 5.20, controller performance for the 2nd mode is represented. In addition, the controller output is also given in Figure 5.21 to show that it is also performing near its physical bounds. Similar procedure is experimented also

for the 3rd mode. Controller performance is shown in Figure 5.22 and the controller output is shown in Figure 5.23.

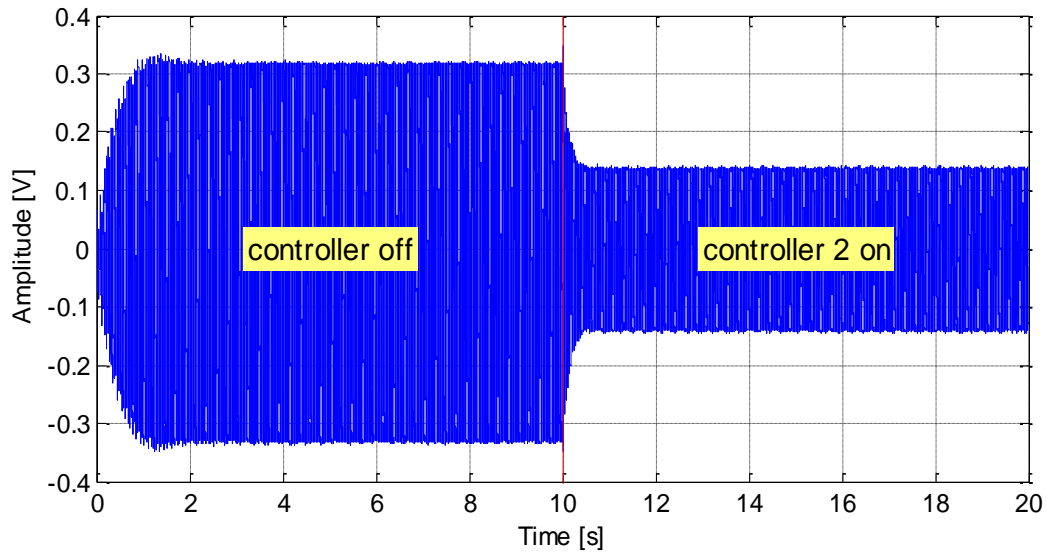


Figure 5.20 Active Vibration Control of the Plate due to an External Force at the 2nd Resonance Frequency

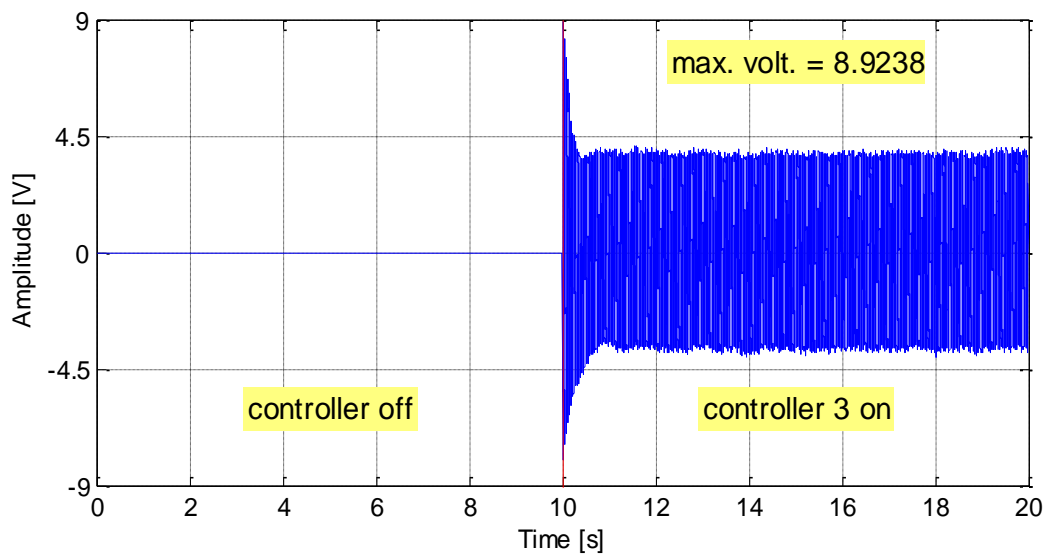


Figure 5.21 Controller Output to Suppress the 2nd Mode Vibration

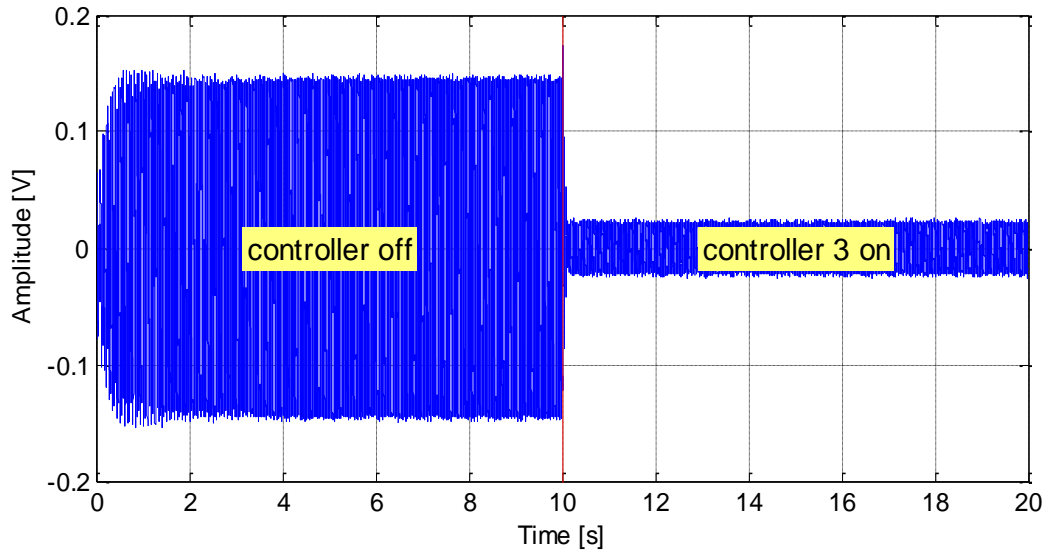


Figure 5.22 Active Vibration Control of the Plate due to an External Force at the 3rd Resonance Frequency

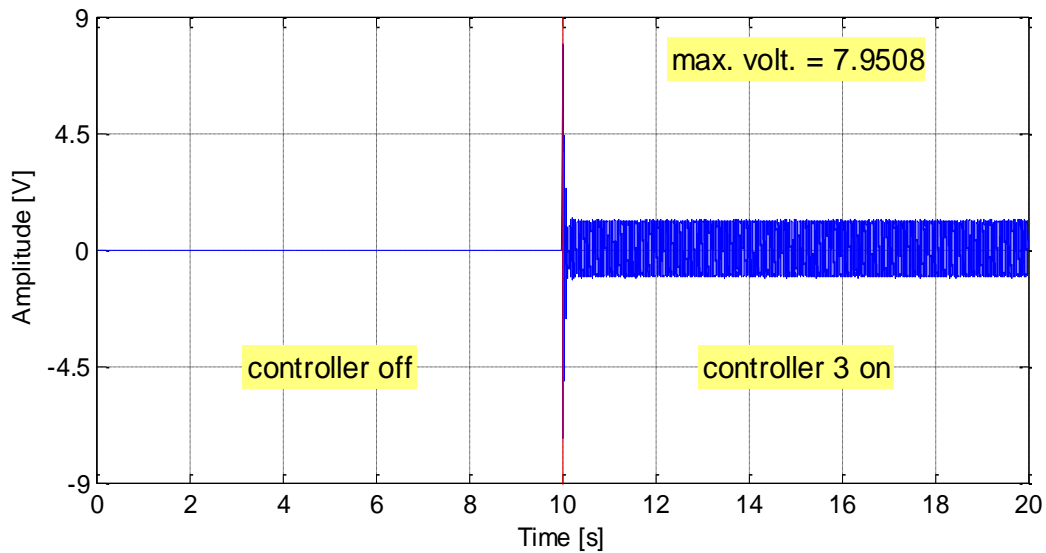


Figure 5.23 Controller Output to Suppress the 3rd Mode Vibration

Figure 5.24, Figure 5.25 and Figure 5.26 show the experimental results for the sinusoidal inputs of 1st, 2nd and 3rd mode of vibration, respectively. After it is ensured that, all of the controllers are working as expected, sinusoidal signals from the disturbance patch are given at the resonance frequencies of the plate in sequence. Controllers endeavor to suppress each of the mode sequentially so as to verify that the controller groups are specialized to their own intended mode. To illustrate, sinusoidal

signal with 4 V is given to excite the system at its specific resonance frequency for 60 seconds. Controller groups 1, 2 and 3 are turned on between 10 – 20 seconds, 30 – 40 seconds and 50 – 60 seconds, respectively. This case is experimented three times for the first three modes to show that the groups are optimized for the specific mode to suppress.

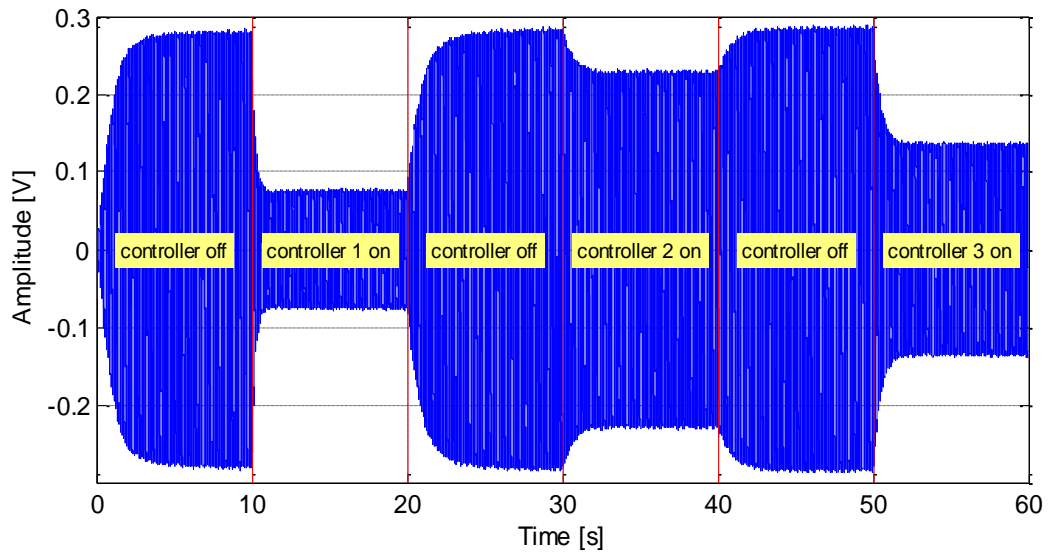


Figure 5.24 Attenuation of the 1st mode via each Controller Groups

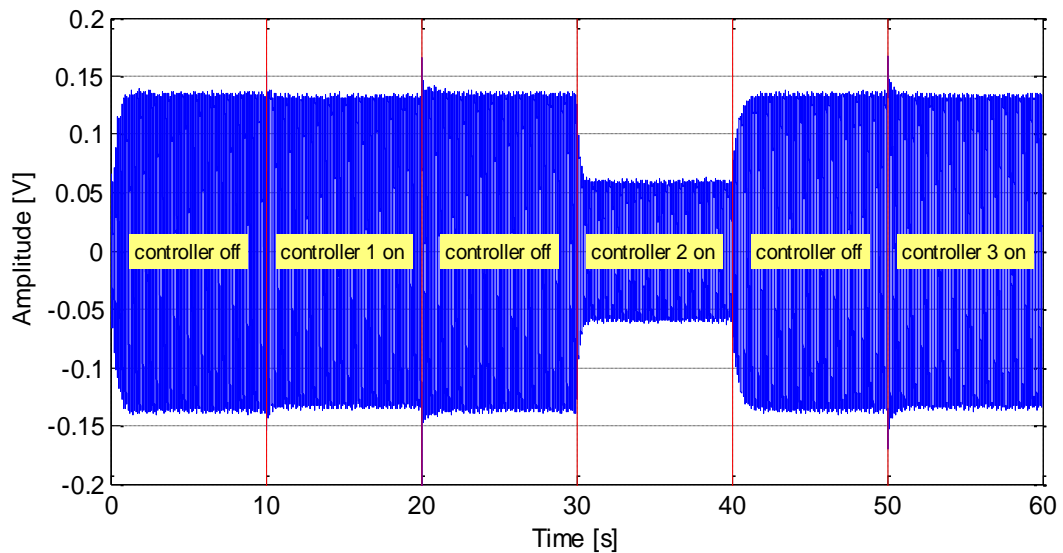


Figure 5.25 Attenuation of the 2nd mode via each Controller Groups

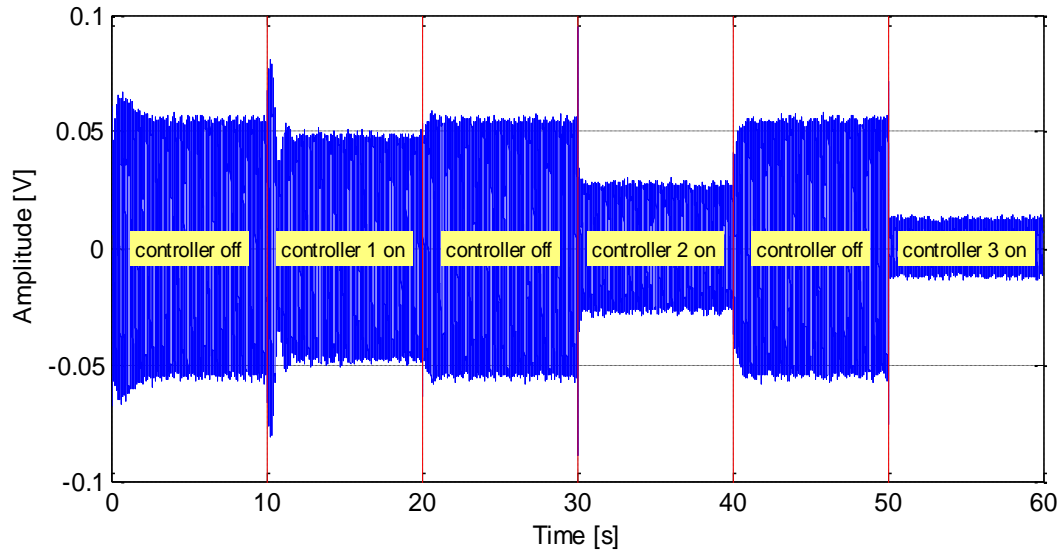


Figure 5.26 Attenuation of the 3rd mode via each Controller Groups

Following these experiments, in order to investigate the performance of the controllers at their corresponding modes as well as for the other modes with a performance loss, it is required to activate all of the controllers at the same time to show that they can work together and suppress the vibrations. For the proof, three experiments are held. In the first case, disturbance at the first resonance frequency with an amplitude of 4 V is given for 40 seconds. From 10th to 20th seconds, only the 1st controller group is activated while from 30th seconds all of the controllers work together (Figure 5.27). Same case is conducted for the 2nd and the 3rd modes by activating 2nd and 3rd controller groups with a disturbance signal at the 2nd and the 3rd resonance frequencies, respectively (Figure 5.28 & Figure 5.29).

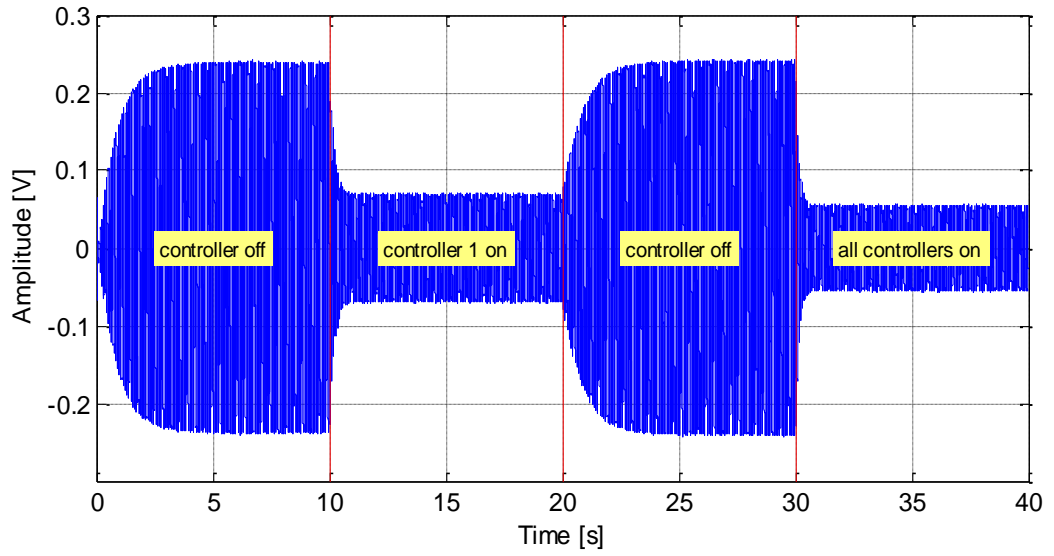


Figure 5.27 Attenuation of the 1st mode via 1st and all Controller Groups

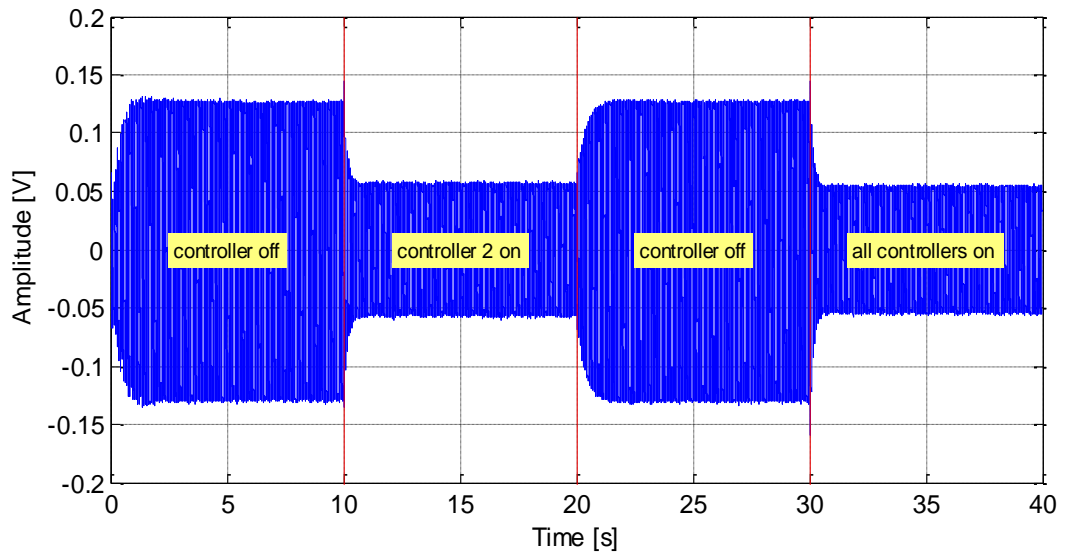


Figure 5.28 Attenuation of the 2nd mode via 2nd and all Controller Groups

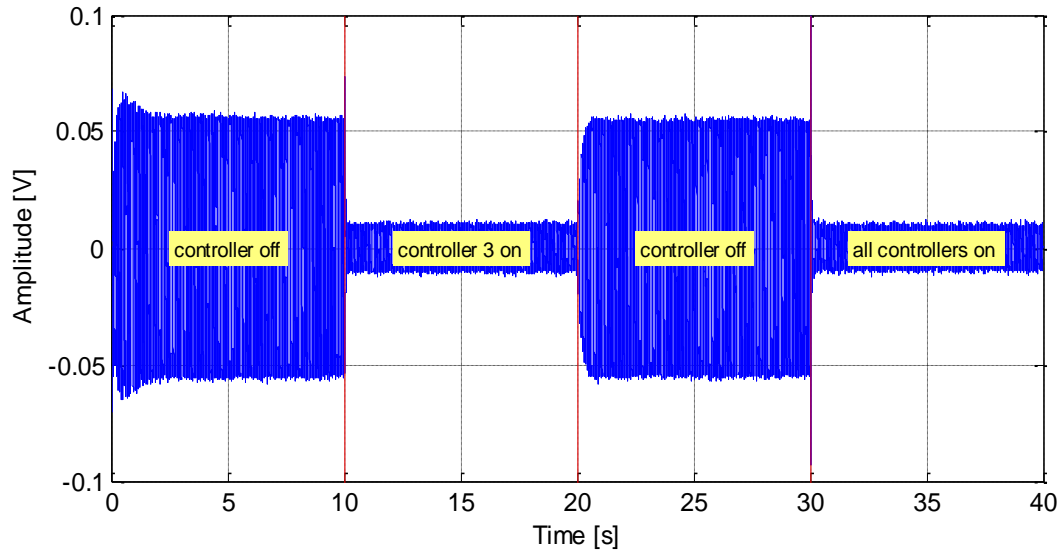


Figure 5.29 Attenuation of the 3rd mode via 3rd and all Controller Groups

5.5.2 Sinusoidal Chirp Signal

In order to see the attenuation levels in dB units, a sine chirp from is given to the plate from the disturbance patch. First it is experimented while the controllers are off. After that, the same chirp is given; however, this time while the controllers are on. Performing Fast Fourier Transform gives the FRFs of both controller on and controller off cases. To compare the couple effects of the controllers to each other, chirp signals are given only activating the corresponding controller of the mode with the frequency intervals of 1 Hz to 20 Hz, 20 Hz to 40 Hz, 55 Hz to 75 Hz, respectively. After the reduction in the dB levels are found for each mode separately, a sine chirp with a frequency interval of 1 to 100 Hz is given. Figure 5.30 shows 1st mode dB levels, Figure 5.31 shows 2nd mode dB levels and Figure 5.32 shows 3rd mode dB levels. Figure 5.33 shows the comparison graph of the responses of the plate for all modes with and without controller cases. Since the results of the separate systems and the combined systems are much closed, one can say that the system is not been affected of the coupling of the modes. This means that the controllers can be used together to suppress vibrations on the plate.

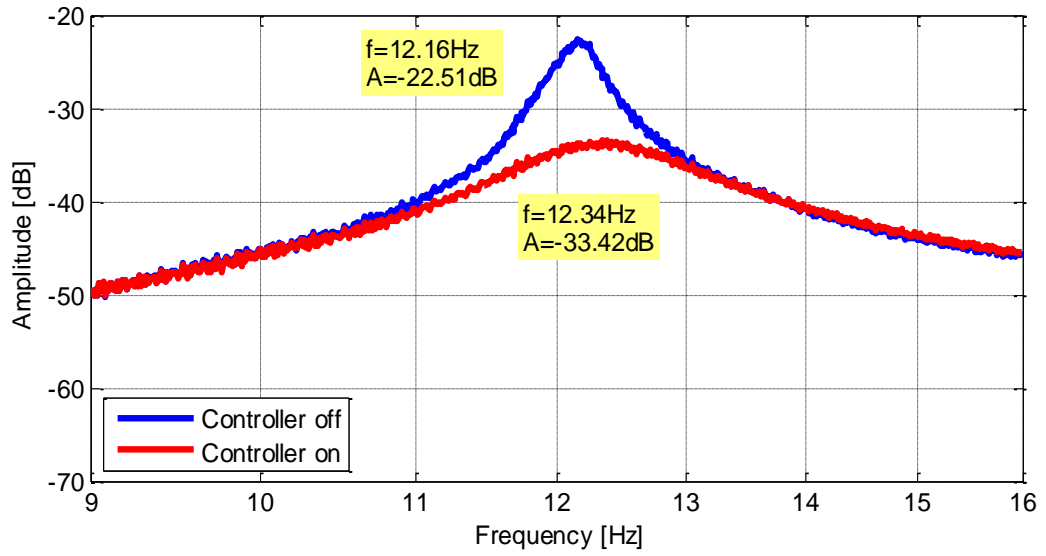


Figure 5.30 Comparison of the System Response of the 1st Mode with and without Controller Group 1

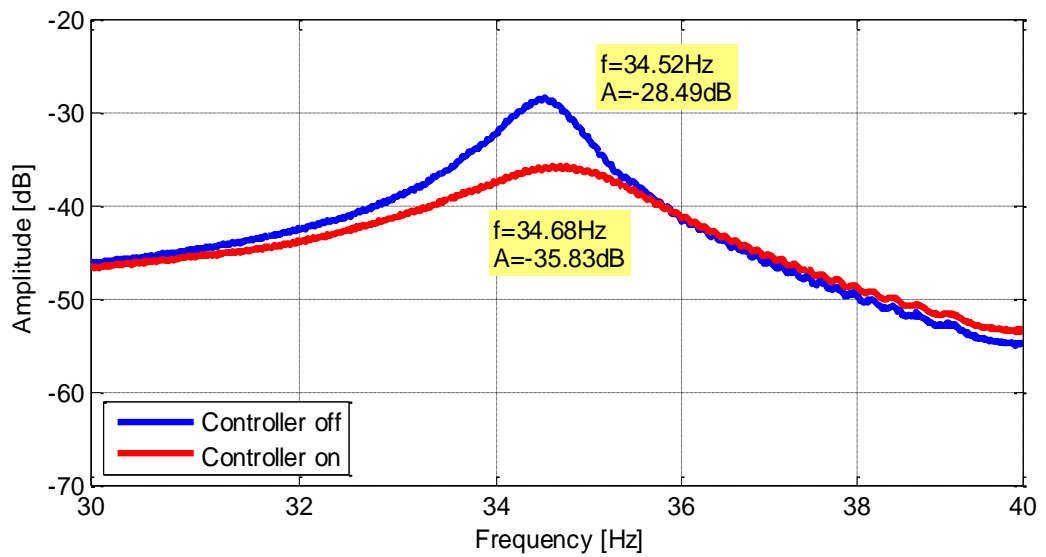


Figure 5.31 Comparison of the System Response of the 2nd Mode with and without Controller Group 2

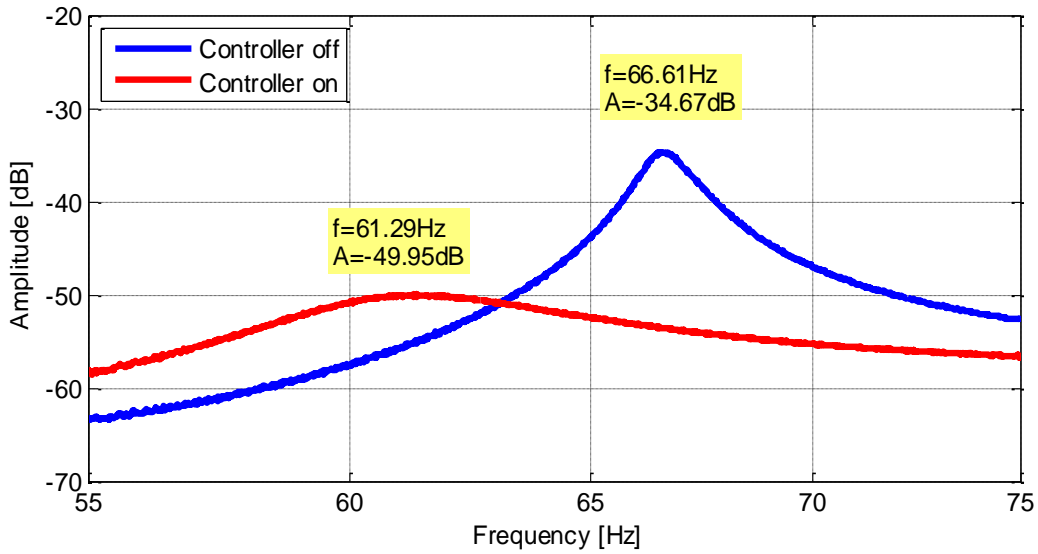


Figure 5.32 Comparison of the System Response of the 3rd Mode with and without Controller Group 3

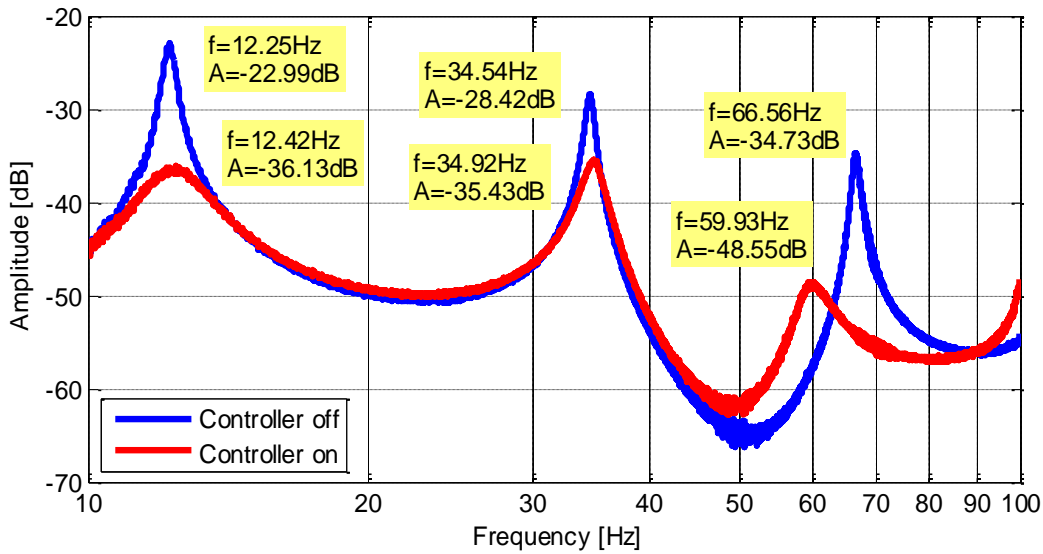


Figure 5.33 Comparison of the System Responses with and without all Controllers

Summation of the results are given in Table 5.5. The first column in the table represents simulation results whereas the last two columns provide information about the experimental outcomes regarding the attenuation due to controllers. The attenuation levels are in close to each other regarding only one controller group is active as well as all groups are active. As the results are in close agreement, it can be

said that the controllers can work together without affecting the others in a compromising way. As it is observed from Figure 5.32 and Figure 5.33, there is a frequency change in the peaks of the 3rd mode. Results of that phenomenon is the filter dynamic at 3rd mode which occurs at relatively high frequency. Nevertheless, the filters cannot be excluded from the system since they are must to have inside the experimental setup boundaries.

Table 5.5 Comparison of Attenuation Levels

	Simulation Results [dB]	Attenuation due to One Controller [dB]	Attenuation due to all Controllers [dB]
Mode 1	10.22	10.91	13.14
Mode 2	7.78	7.34	7.01
Mode 3	12.73	15.28	13.82

5.6 Conclusion

In this chapter, piezoelectric patches are used for active vibration control of the smart sandwich plate. First of all the controllers are designed and the system simulations are performed to verify that the controllers are working properly within the physical limits of the hardware used. Following these, experiments are conducted to show that the controllers are effective to suppress vibrations in real life scenarios. When the experiments are completed, the results are then compared with that of the simulations and it is seen that they are in good agreement with each other. In free vibration case full suppression of the vibration takes approximately 5 seconds at the open loop where full suppression of the closed loop vibration takes less than 1 second. On the other hand, in the forced vibration case, response to the chirp signal decrease 10 dB for the first mode, 7 dB for the second mode and 15 dB for the third mode because of the controllers which are working together. This means that, separately designed single input single output controllers are working together without coupling effects which causes rise in modes other than the controlling modes. In fact, for the

first mode, combined controllers perform better. All in all, this experimental work shows how the controllers react effectively.

CHAPTER 6

CONCLUSIONS

6.1 General Conclusions

In this thesis, an active vibration control of a smart sandwich plate is studied. For both controlling and sensing purposes, surface bonded piezoelectric patches are used.

First of all, the sandwich plate is modelled using finite element methods. After the model of the plate is generated and the analyses are performed, an experimental verification is done to have more accurate model. The mode shapes obtained from this model are then used to locate the piezoelectric patches on a passive sandwich plate. An algorithm using maximum curvature locations in the first three modes which also correspond to the maximum strain location are adapted. First, two PZT patches each of which is responsible from sensing and creating disturbance are placed. Finally, all the controller patches are located over the surface of the plate. After this piezoelectric patch attachment procedure, the sandwich plate is called as “Smart Sandwich Plate”.

Following all the numerical analyses, the vibration characteristics of the smart sandwich plate are investigated through a sine chirp signal given as an input to the system in order to excite all the frequencies within the interval of interest. Then, the frequency response functions for input output pairs of each controller groups are obtained experimentally and transfer functions associated to this frequency response functions are fitted.

Having completed the system model estimation, pole placement type controller is designed to raise the damping ratio of the system. Since the pole placement controller needs the system states to be measured which are not available, system observers are also designed. In order to develop the performance of the controllers, band pass filters are implemented and the controller gains are tuned together with those filters. Those controllers are examined through simulations to adjust parameters and to affirm the performances. For the verification of the controllers in the vibration suppression of the first three modes of smart sandwich plate, they are tested separately through various experiments. After the observation of their individual performance, the combination of all the controllers are also tested. It is found that the degradation in vibration levels represented in frequency domain regarding the performance of an individual and combined controllers are close to each other although slightly better performance is achieved in the case where three controllers are used together as a group.

As a result, in this thesis study, it is shown that the piezoelectric patch groups located regarding the maximum curvature of the vibrational modes of a sandwich plate structure can be used with designed controllers to suppress the intended modes actively in an efficient manner.

6.2 Recommendation for Future Work

In this study, three single input single output pole placement type controllers are implemented together to control the vibrations in the three modes of the smart sandwich plate.

In order to improve this work following suggestions may be offered:

- Different types of controllers may be tried to compare the performance.
- Multi-input and multi-output controller systems may be designed.
- Adaptive controllers may be designed to improve the performance of the vibration suppression.

- Advanced controllers may be implemented to have both better performance in a broader frequency range.

Performance of the controllers may be observed under aerodynamic loads with possible wind tunnel applications under real life scenarios.

REFERENCES

- [1] T. Bitzer, *Honeycomb Technology: Materials, Design, Manufacturing, Applications And Testing*. 1997.
- [2] Y. Li, X. Wang, R. Huang, and Z. Qiu, “Active vibration and noise control of vibro-acoustic system by using PID controller,” *J. Sound Vib.*, vol. 348, pp. 57–70, 2015.
- [3] D. Halim, X. Luo, and P. M. Trivailo, “Decentralized vibration control of A multi-link flexible robotic manipulator using smart piezoelectric transducers,” *Acta Astronaut.*, vol. 104, no. 1, pp. 186–196, 2014.
- [4] S. Thenozhi and W. Yu, “Stability analysis of active vibration control of building structures using PD/PID control,” *Eng. Struct.*, vol. 81, pp. 208–218, 2014.
- [5] M. Jafari and H. Djojodihardjo, “Vibration Control of an Elastic Structure using Piezoelectric Sensor and Actuator with Cantilevered Beam as a Case Study,” in *Scientific Cooperations International Workshops on Electrical and Computer Engineering Subfields, Koc University*, 2014, pp. 218–226.
- [6] R. Dubay, M. Hassan, C. Li, and M. Charest, “Finite element based model predictive control for active vibration suppression of a one-link flexible manipulator,” *ISA Trans.*, vol. 53, no. 5, pp. 1609–1619, 2014.
- [7] D. Wu, L. Huang, B. Pan, Y. Wang, and S. Wu, “Experimental study and numerical simulation of active vibration control of a highly flexible beam using piezoelectric intelligent material,” *Aerosp. Sci. Technol.*, vol. 37, pp. 10–19, 2014.
- [8] M. Kerboua, a. Megnounif, M. Benguediab, K. H. Benrahou, and F. Kaoulala, “Vibration control beam using piezoelectric-based smart materials,” *Compos. Struct.*, vol. 123, pp. 430–442, 2015.
- [9] A. Zippo, G. Ferrari, M. Amabili, M. Barbieri, and F. Pellicano, “Active vibration control of a composite sandwich plate,” *Compos. Struct.*, vol. 128, pp. 100–114, 2015.
- [10] K. Chevva, F. Sun, A. Blanc, and J. Mendoza, “Active vibration control using minimum actuation power,” *J. Sound Vib.*, vol. 340, pp. 1–21, 2015.

- [11] Y. Luo, S. Xie, and X. Zhang, "Vibration control of honeycomb sandwich panel using multi-layer piezoelectric actuator," *Comput. Struct.*, vol. 86, no. 7–8, pp. 744–757, 2008.
- [12] Y. Luo, S. Xie, and X. Zhang, "The actuated performance of multi-layer piezoelectric actuator in active vibration control of honeycomb sandwich panel," *J. Sound Vib.*, vol. 317, no. 3–5, pp. 496–513, 2008.
- [13] Z.-G. Song and F.-M. Li, "Optimal locations of piezoelectric actuators and sensors for supersonic flutter control of composite laminated panels," *J. Vib. Control*, no. January, 2013.
- [14] A. R. Damanpack, M. Bodaghi, M. M. Aghdam, and M. Shakeri, "Active control of geometrically non-linear transient response of sandwich beams with a flexible core using piezoelectric patches," *Compos. Struct.*, vol. 100, pp. 517–531, 2013.
- [15] S. Belouettar, L. Azrar, E. M. Daya, V. Laptev, and M. Potier-Ferry, "Active control of nonlinear vibration of sandwich piezoelectric beams: A simplified approach," *Comput. Struct.*, vol. 86, no. 3–5, pp. 386–397, 2008.
- [16] B. P. Baillargeon, "Active Vibration Suppression of Sandwich Beams using Piezoelectric Shear Actuators: Experiments and Numerical Simulations," *J. Intell. Mater. Syst. Struct.*, vol. 16, no. 6, pp. 517–530, 2005.
- [17] R. Suresh and G. V. Rao, "Simple analytical solution for active vibration control of intelligent composite and sandwich plates," *Indian J. Eng. Mater. Sci.*, vol. 12, no. June, pp. 196–206, 2005.
- [18] G. Ferrari and M. Amabili, "Active vibration control of a sandwich plate by non-collocated positive position feedback," *J. Sound Vib.*, vol. 342, pp. 44–56, 2015.
- [19] S. Raja, S. Janardhanam, V. Shankar, B. Balakrishnan, K. R. Rekha, and A. K. Asraff, "Implementation of an Active Vibration Control Technique on a Full Scale Space Vehicle Structure," *Inst. Smart Struct. Syst.*, vol. 1, no. 1, pp. 46–54, 2012.
- [20] D. Zenkert, *An Introduction to Sandwich Construction*. Engineering Materials Advisory Services, 1995.
- [21] D. Zenkert, *The Handbook of Sandwich Construction*. Eastbourne: Antony Rowe Ltd, 1997.
- [22] J. Kindinger, "Lightweight Structural Cores," *ASM Handb. Met. Vol. 21-Composites*, vol. 3, 2001.

- [23] J. K. Ajitsaria, “Modeling And Analysis Of PZT Micropower Generator,” Auburn University, 2008.
- [24] Piezokeramika European Piezo Ceramics, “Piezoelectricity,” 2008. [Online]. Available: <http://piezokeramika.wcz.cz/piezo.php?vek=8>. [Accessed: 21-Jul-2015].
- [25] Q.-H. Qin, *Advanced Mechanics of Piezoelectricity*. 2012.
- [26] C. Gençoğlu, “Active Vibration Control of Beams and Cylindrical Structures Using Piezoelectric Patches,” Middle East Technical University, 2014.
- [27] W. Heywang, K. Lubitz, and W. Wersing, *Piezoelectricity: Evolution and Future of a Technology*. 2008.
- [28] J. Yang, *An Introduction to the Theory of Piezoelectricity*. Boston: Springer Science + Business Media Inc., 2005.
- [29] A. Mallock, “A Method of Preventing Vibration in Certain Classes of Steamships,” *Trans. R. Inst. Nav. Archit.*, vol. 47, pp. 227–230, 1905.
- [30] S. Daley, F. A. Johnson, J. B. Pearson, and R. Dixon, “Active vibration control for marine applications,” *Control Eng. Pract.*, vol. 12, no. 4, pp. 465–474, 2004.
- [31] K. Kowalczyk and F. Svaricek, “An Overview of Recent Automotive Applications of Active Vibration Control,” in *Habitability of Combat and Transport Vehicles: Noise, Vibration and Motion*, 2004, no. 24.
- [32] D. Guicking and T. Kurz, “Active control of sound and vibration: History–fundamentals–state of the art,” *Oscil. Waves ...*, pp. 51–58, 2007.
- [33] O. Tokhi and S. M. Veres, *Active Sound and Vibration Control: Theory and Applications*. London: Institution of Electrical Engineers, 2002.
- [34] M. Itik, M. U. Salamci, F. D. Ulker, and Y. Yaman, “Active Vibration Suppression of a Flexible Beam via Sliding Mode,” in *Proceedings of the 44th IEEE Conference on Decision and Control, and the European Control Conference*, 2005, pp. 1240–1245.
- [35] Ö. F. Kircali, Y. Yaman, V. Nalbantoğlu, and M. Şahin, “Active Vibration Control of a Smart Beam by Using a Spatial Approach,” in *New Developments in Robotics Automation and Control*, I-Tech Education and Publishing, 2008, pp. 377–410.

- [36] Y. Chen, F. D. Ulker, V. Nalbantoglu, V. Wickramasinghe, D. Zimcik, and Y. Yaman, "Active Control of Smart Fin Model for Aircraft Buffeting Load Alleviation Applications," *J. Aircr.*, vol. 46, no. 6, pp. 1965–1972, 2009.
- [37] C. Onat, M. Şahin, and Y. Yaman, "Fractional controller design for suppressing smart beam vibrations," *Aircr. Eng. Aerosp. Technol.*, vol. 84, no. 4, pp. 203–212, 2012.
- [38] C. Onat, M. Şahin, and Y. Yaman, "An Experimental Performance Evaluation for the Suppression of Vibrations of the Second Mode of a Smart Beam," in *6. Ankara International Aerospace Conference*, 2011.
- [39] M. Sahin, F. M. Karadal, Y. Yaman, O. F. Kircali, V. Nalbantoglu, F. D. Ulker, and T. Caliskan, "Smart structures and their applications on active vibration control: Studies in the Department of Aerospace Engineering, METU," *J. Electroceramics*, vol. 20, no. 3–4, pp. 167–174, 2008.
- [40] T. Çalışkan, "Piezoelectric Ceramics and Their Applications in Smart Aerospace Structures," Middle East Technical University, 2002.
- [41] C. Onat, M. Sahin, and Y. Yaman, "Optimal Control of a Smart Beam by using a Luenberger Observer," in *3rd International Conference of Engineering Against Failure (ICEAF III)*, 2013, pp. 804–811.
- [42] C. Onat, M. Sahin, and Y. Yaman, "Active Vibration Suppression of a Smart Beam by Using an LQG Control Algorithm," in *2nd International Conference of Engineering Against Fracture (ICEAF II)*, 2011.
- [43] F. D. Ülker, V. Nalbantoğlu, Y. Chen, D. Zimcik, and Y. Yaman, "Active Vibration Control of a Smart Fin," in *50th AIAA/ASME/ASCE/AHS/ASC Structures, Structural Dynamics, and Materials Conference*, 2009.
- [44] "Patran Complete FEA Modeling Solution," 2015. [Online]. Available: <http://www.mscsoftware.com/product/patran>. [Accessed: 29-Jun-2015].
- [45] "MSC Nastran Multidisciplinary Structural Analysis," 2015. [Online]. Available: <http://www.mscsoftware.com/product/msc-nastran>. [Accessed: 29-Jun-2015].
- [46] Brüel&Kjær, "Accelerometers & Conditioning Product Catalogue." 2009.
- [47] "PULSE Modal Test Consultant Type 7753," 2015. [Online]. Available: <http://www.bksv.com/products/analysis-software/vibration/structural-dynamics/classical-modal-analysis/modal-test-consultant-7753>. [Accessed: 15-Mar-2015].

- [48] M. Pastor, M. Binda, and T. Harčarik, “Modal assurance criterion,” *Procedia Eng.*, vol. 48, pp. 543–548, 2012.
- [49] FEMtools, “Dynamic Design Solutions,” 2015. [Online]. Available: <http://www.femtools.com/products/ftmu.htm>. [Accessed: 29-Jun-2015].
- [50] I. Bruant, L. Gallimard, and S. Nikoukar, “Optimal piezoelectric actuator and sensor location for active vibration control, using genetic algorithm,” *J. Sound Vib.*, vol. 329, no. 10, pp. 1615–1635, 2010.
- [51] V. Gupta, M. Sharma, and N. Thakur, “Optimization Criteria for Optimal Placement of Piezoelectric Sensors and Actuators on a Smart Structure: A Technical Review,” *J. Intell. Mater. Syst. Struct.*, vol. 21, no. 12, pp. 1227–1243, 2010.
- [52] Z. N. Li, J. Tang, and Q. S. Li, “Optimal sensor locations for structural vibration measurements,” *Appl. Acoust.*, vol. 65, no. 8, pp. 807–818, 2004.
- [53] J. Z. J. Zhang, L. H. L. He, E. W. E. Wang, and R. G. R. Gao, “A LQR Controller Design for Active Vibration Control of Flexible Structures,” *2008 IEEE Pacific-Asia Work. Comput. Intell. Ind. Appl.*, vol. 1, pp. 128–133, 2008.
- [54] Sensor Technologies Limited., “BM-500 Lead Zirconate Titanate Product Data Sheet.” 2002.
- [55] Bison, “Epoxy Metal.” [Online]. Available: <http://www.bison.net/en/products/647-2-components-adhesives/product/2273-epoxy-metal/>. [Accessed: 06-Jul-2015].
- [56] MathWorks - Speedgoat - System Integration Services, “Speedgoat - System Integration Services,” 2015. [Online]. Available: http://www.mathworks.com/products/connections/product_detail/service_35987.html. [Accessed: 10-Jul-2015].
- [57] Sensor Technology Limited., “Sensor Product Overview.” 2006.
- [58] G. J. Balas, J. C. Doyle, K. Glover, A. Packard, and R. Smith, “Mu Analysis and Synthesis Toolbox For Use with MATLAB.” MathWorks, Inc., Natick, 2001.
- [59] K. Ogata, *Discrete Time Control Systems*. New Jersey: Prentice-Hall, Inc., 1995.
- [60] K. Ogata, *Modern Control Engineering*. New Jersey: Prentice-Hall, Inc., 2002.